Sussex Research Online

Classification of parameter spaces for a reaction-diffusion model on stationary domains

Article (Published Version)

Sarfaraz, Wakil and Madzvamuse, Anotida (2017) Classification of parameter spaces for a reaction-diffusion model on stationary domains. Chaos, Solitons & Fractals, 103. pp. 33-51. ISSN 0960-0779

This version is available from Sussex Research Online: http://sro.sussex.ac.uk/68348/

This document is made available in accordance with publisher policies and may differ from the published version or from the version of record. If you wish to cite this item you are advised to consult the publisher's version. Please see the URL above for details on accessing the published version.

Copyright and reuse:
Sussex Research Online is a digital repository of the research output of the University.

Copyright and all moral rights to the version of the paper presented here belong to the individual author(s) and/or other copyright owners. To the extent reasonable and practicable, the material made available in SRO has been checked for eligibility before being made available.

Copies of full text items generally can be reproduced, displayed or performed and given to third parties in any format or medium for personal research or study, educational, or not-for-profit purposes without prior permission or charge, provided that the authors, title and full bibliographic details are credited, a hyperlink and/or URL is given for the original metadata page and the content is not changed in any way.

http://sro.sussex.ac.uk

Chaos, Solitons and Fractals 103 (2017) 33–51

Contents lists available at ScienceDirect

Chaos, Solitons and Fractals

Nonlinear Science, and Nonequilibrium and Complex Phenomena

journal homepage: www.elsevier.com/locate/chaos

Classification of parameter spaces for a reaction-diffusion model on stationary domains

Wakil Sarfaraz*, Anotida Madzvamuse*

University of Sussex, School of Mathematical and Physical Sciences, Department of Mathematics, Pevensey 3, Brighton, BN1 9QH, UK

ARTICLE INFO

Article history:
Received 7 January 2017
Revised 3 May 2017
Accepted 25 May 2017

Keywords:
Reaction-diffusion systems
Dynamical systems
Bifurcation analysis
Stability analysis
Turing diffusion-driven instability
Hopf bifurcation
Transcritical bifurcation
Parameter spaces

ABSTRACT

This paper explores the classification of parameter spaces for reaction-diffusion systems of two chemical species on stationary rectangular domains. The dynamics of the system are explored both in the absence and presence of diffusion. The parameter space is fully classified in terms of the types and stability of the uniform steady state. In the absence of diffusion the results on the classification of parameter space are supported by simulations of the corresponding vector-field and some trajectories of the phase-plane around the uniform steady state. In the presence of diffusion, the main findings are the quantitative analysis relating the domain-size with the reaction and diffusion rates and their corresponding influence on the dynamics of the reaction-diffusion system when perturbed in the neighbourhood of the uniform steady state. Theoretical predictions are supported by numerical simulations both in the presence as well as in the absence of diffusion. Conditions on the domain size with respect to the diffusion and reaction rates are related to the types of diffusion-driven instabilities namely Turing, Hopf and Transcritical types of bifurcations. The first condition is a lower bound on the area of a rectangular domain in terms of the diffusion and reaction rates, which is necessary for Hopf and Transcritical bifurcation to occur. The second condition is an upper bound on the area of domain in terms of reaction-diffusion rates that restricts the diffusion-driven instability to Turing type behaviour, whilst forbidding the existence of Hopf and Transcritical bifurcation. Theoretical findings are verified by the finite element solution of the coupled system on a two dimensional rectangular domain.

© 2017 Published by Elsevier Ltd.

1. Introduction and model equations

1.1. Introduction

Reaction-diffusion systems (RDSs) attract a significant degree of attention from researchers in applied mathematics [1–9], mathematical and computational biology [10–14], chemical engineering [15–17] and so forth. Alan Turing was one of the first scientists to realise the significance of RDSs as a self-governing dynamical system [18], and showed that RDSs can be responsible for the emergence of spatial patterns in nature. A large number of scientists [1,2,8,11,19–21], since the publication of Turing [18], have contributed to investigating RDSs, with various types of reaction kinetics. The most popular models of reaction kinetics explored in the literature are the *activator-depleted* model (also known as the Schnakenberg reaction kinetics) [2,20,22–24], Meinhardt [12,13] and Thomas [25] reaction kinetic models. From a research perspective the study of RDSs is conducted through different types of approaches, one of which focuses on the local behaviour of the dynamics of the RDS near a uniform steady state, which in turn relates to the subject of stability analysis [6,8,12,20,26,27] of RDSs using the stability matrix. Linear stability analysis offers a great deal of insight regarding the behaviour of RDSs in the neighbourhood of a uniform steady state of a particular system. The other usual approach is numerical computation of the actual solution of RDSs using finite element, finite difference and other numerical methods [1,2,4,5,7,9,28–30]. Numerical solution of RDSs helps to visualise the evolution of the dynamics in time. Numerical computations of RDSs with non-linear reaction kinetics with a particular choice of parameters partially encapsulates the possible types of dynamics that a certain RDS can exhibit. In order to better understand the behaviour of RDSs, it is necessary to have prior knowledge on the classification of the parameter values. Madzvamuse et al., in [20,27] found regions of parameter space, corresponding to diffusion-driven instability with and without cross-diffusion respectively using the well-known *activator-depleted* reaction kinetics. Their approach to finding unstable regions in the parameter

* Corresponding authors. Tel.: +447832903102.
E-mail addresses: wakilsarfaraz@gmail.com, ws49@sussex.ac.uk (W. Sarfaraz), A.Madzvamuse@sussex.ac.uk (A. Madzvamuse).

http://dx.doi.org/10.1016/j.chaos.2017.05.032
0960-0779/© 2017 Published by Elsevier Ltd.

space is restricted to Turing instability only. One of the few complementary contributions from the present work is the application of a numerical method (exclusive to this paper) in order to obtain the full classification of parameter space. The numerical method is also employed to solve the equations for the implicit curves forming the partitioning of the classification within the parameter space. Iron et al., present a detailed study in [28] on the stability analysis of Turing patterns generated by *activator-depleted* reaction kinetics in one spatial dimension. Despite the presentation of rigorous and well-demonstrated proofs in [28], their results are restricted to spatial patterns with focus on the emergence of the number of spatial peaks relative to the eigenvalues of the one-dimensional diffusion operator. Xu and Wei investigated *activator-depleted* reaction-diffusion model in [31] with restriction to one spatial dimension focusing mainly on Hopf bifurcation. The approach in [31] is not aimed to produce any results that relate the domain size (length) to the reaction-diffusion rates. Yi *et al.* studied bifurcation analysis and spatiotemporal patterns of a diffusive predator-prey system in one space dimension [32]. The results obtained in [32] are mainly theoretical with limited numerical demonstration and in comparison with the current work, no attention is given to analyse whether domain size have any role in the bifurcation behaviour of the system in [32]. Reaction-diffusion system with *activator-depleted* reaction kinetics is investigated in [33] with time delay in one-dimensional space and it is theoretically proven with limited numerical verifications that Hopf bifurcation can occur with given constraints on the parameter values of the system. Liu *et al.*, in [34] attempted to find constraints on the parameters of RDSs with *activator-depleted* reaction kinetics that causes the system to exhibit Hopf and transcritical bifurcations. The proofs in [34] are focused on the existence of bifurcation points for some theoretical constraints of parameterised variables of the actual parameters, with no relation between the domain size and reaction-diffusion rates. Comparing their work to the present study, our results are robust in the sense that we explicitly relate domain size to the reaction-diffusion rates. Using this relationship, the parameter space is classified for different types of bifurcations. Moreover, in the present work the parameter constraints are a consequence of the relationship between the domain size and the reaction-diffusion rates. An additional drawback in the analysis of Liu et al. [34] is that their results are produced on parameterised variables of the model and not on the actual parameters of the equations, which makes their results applicable to non-realistic possibilities (negative values) of the actual parameters of the model. This drawback is effectively resolved in the current work as the analysis is conducted on the actual two-dimensional positive real parameter space, which in addition to confirming the existence of different bifurcation regions, it offers concrete quantitative classification of the parameter space that guarantees the dynamics of RDSs to exhibit these bifurcations.

The majority of RDSs in the literature [2,3,9,19,21,35] that exhibit spatial or temporal pattern, contain nonlinear terms in their reaction kinetics, which makes the mathematical and numerical analysis of such systems extremely challenging. With no closed analytical solutions, studies of the local behaviour of the systems are generally conducted by use of linear stability theory close to bifurcation points. Here, the behaviour of a system can be theoretically predicted in the neighbourhood of the uniform steady states. Linear stability analysis can help derive certain conditions on the reaction kinetics, which lead to causing instability in the dynamics of RDSs in the presence of diffusion. Numerous papers [6,8,20,24,27] exist in literature that routinely apply linear stability analysis to RDSs. A routinely used approach related to stability analysis of RDSs [6,24,27,31,32] focuses on deriving linear stability conditions in terms of the characteristics of the stability matrix for diffusion-driven instability, lacking to explore what the numerical application of these conditions induce on the admissible choice of the parameter space for a certain RDS. Spatio-temporal pattern formation occurs when an RDS undergoes diffusion-driven instability [18,23,36]. This occurs when a uniform steady state which is stable in the absence of diffusion becomes unstable upon adding diffusion to the system. Diffusion-driven instability crucially depends on the values of diffusion and reaction rates of each reactant, however, more importantly it depends on the parameter choice of the reaction kinetics. In the current work the existing knowledge on the conditions for diffusion-driven instability in the literature is extended using a series of analytical and numerical techniques, to obtain new insights on the combined effects of diffusion and reaction rates, and in turn relating these to domain size of the evolution of the pattern. The detailed and quantitative analysis on the relationship between the domain size and diffusion-reaction rates in light of the parameter classification is an aspect that has not been studied in the literature. The usual approach in selecting parameters for numerical computations of RDSs [14,36] is based on the behaviour of RDSs in the absence of diffusion by use of trial and error or is based on previously published work, to observe instability caused by diffusion [1,2,6,9,19]. The absence of a robust method to fully classify the parameter space for an RDS, creates an arguable platform for the importance of this work. Efficient analytical as well as computational methods are used to demonstrate the quantitative relationship between the domain size and diffusion rate for an *activator-depleted* RDS. The main findings of the present work, which relate the domain size to the diffusion and reaction rates, are presented in the form of theorems with rigorous mathematical proofs and these theoretical results are supported computationally by finite element numerical solutions corresponding to the *activator-depleted* RDS on fixed rectangular domains. For each numerical demonstration the relative error plots of the solutions for each successive time-step are presented to visualise the convergence of the numerical approximate solutions.

This article is therefore structured as follows. In Section 1.2 we state model equations with the corresponding initial and boundary conditions. Section 2 presents a detailed theoretical linear stability analysis of the system (1) in the absence of diffusion. Linear stability analysis is conducted by computing the stability matrix through which, the non-dimensional parameter space is derived and classified. Section 2.3 presents the methodology to compute the solutions of the partitioning curves for the classification on the parameter space. A combination of analytical and numerical methods using polynomials are applied. In Section 3, the linear stability analysis of the system is conducted in the presence of diffusion and the parameter space is explored to understand the consequences of including diffusion in the analysis. The parameter space is further explored to find the change in regions of the parameter space through varying the non-dimensional diffusion coefficient. Section 4 contains the finite element solution of system (1), where the theoretical predictions proposed by the linear stability theory subject to conditions on the domain size and parameter spaces are numerically verified. Section 5 presents conclusions, future directions and possible extensions of the current work.

1.2. Model equations

The dynamics of two chemical species u and v in a coupled system of nonlinear parabolic equations is considered. Both species diffuse with independent rates and satisfy the well-known *activator-depleted* reaction-diffusion system in a closed two-dimensional rectangular domain denoted by $\Omega \subset \mathbb{R}^2$ with area $L_x \times L_y$, where L_x and L_y are the corresponding side lengths in the direction of x and y axes respectively. The reaction-diffusion system satisfying the *activator-depleted* model for u and v in its non-dimensional form with Neumann boundary conditions and positive

bounded initial conditions [2,20,23,24] reads as

$$\begin{cases} \begin{cases} \dfrac{\partial u}{\partial t} = \triangle u + \gamma(\alpha - u + u^2 v), & (x,y) \in \Omega, \quad t > 0, \\ \dfrac{\partial v}{\partial t} = d\triangle v + \gamma(\beta - u^2 v), \end{cases} \\ \dfrac{\partial u}{\partial \boldsymbol{n}} = \dfrac{\partial v}{\partial \boldsymbol{n}} = 0, \quad \text{on} \quad (x,y) \in \partial\Omega, \quad t \geq 0, \\ u(x,y,0) = u_0(x,y), \quad v(x,y,0) = v_0(x,y), \\ \quad (x,y) \in \Omega, \quad t = 0, \end{cases} \tag{1}$$

where d, γ, α and β are non-dimensional positive constants and $\boldsymbol{n}$ denotes the outward normal to $\partial\Omega$. In (1) the non-dimensional parameter d denotes the quantity $\frac{D_v}{D_u}$, where D_u is the diffusion rate of the variable u and D_v is the diffusion rate of the variable v. The non-dimensional parameter γ denotes the reaction rate, which is also known as the scaling parameter for the reaction kinetics.

1.2.1. Remark

Despite the fact that all the results obtained in this paper hold for general rectangular geometries of Ω i.e. with possibilities $L_x \neq L_y$, however for simplicity in the analysis Ω is considered as a square, which means $L_x = L_y$. The results can be readily extended to a rectangular case by taking the area of Ω as L^2, where $L = \max\{L_x, L_y\}$.

2. Stability analysis in the absence of diffusion

Despite the fact that the dynamical behaviour of system (2) is a well studied area of research [23,37,38], however the purpose to reproduce these known results is the demonstration of a numerical method in Section 2.3 exclusive to the current work, which can be readily generalised as a robust framework to fully classify parameter spaces for other dynamical systems. In the absence of diffusion the system (1) takes the form of a set of ordinary differential equations of the form

$$\begin{cases} \dfrac{du}{dt} = \gamma(\alpha - u + u^2 v) = \gamma f(u,v), \\ \dfrac{dv}{dt} = \gamma(\beta - u^2 v) = \gamma g(u,v). \end{cases} \tag{2}$$

To analyse the stability of system (2), it is necessary to compute its uniform steady state solution, which is given by $(u_s, v_s) = (\alpha + \beta, \frac{\beta}{(\alpha+\beta)^2})$, satisfying $f(u,v) = g(u,v) = 0$. This enforces a restriction on parameters α and β, that they simultaneously cannot become zero.

The stability of system (2) is analysed by computing the Jacobian matrix of (2) and conducting the stability analysis using the uniform steady state solution (u_s, v_s), hence

$$\boldsymbol{J}|_{(u_s,v_s)} = \gamma \begin{bmatrix} \dfrac{\partial f}{\partial u} & \dfrac{\partial f}{\partial v} \\ \dfrac{\partial g}{\partial u} & \dfrac{\partial g}{\partial v} \end{bmatrix}_{(u_s,v_s)} = \gamma \begin{bmatrix} \dfrac{\beta-\alpha}{\alpha+\beta} & (\beta+\alpha)^2 \\ -\dfrac{2\beta}{\beta+\alpha} & -(\beta+\alpha)^2 \end{bmatrix},$$

which is called the stability matrix [23,37,38] for system (2). Let $T(\alpha,\beta) = \gamma\left(\frac{\beta-\alpha-(\beta+\alpha)^3}{\beta+\alpha}\right)$ and $D(\alpha,\beta) = \gamma^2(\alpha+\beta)^2$ denote the trace and determinant of $\boldsymbol{J}$ respectively, then the characteristic polynomial for the eigenvalues $\lambda_{1,2}$ of $\boldsymbol{J}$ in terms of $T(\alpha,\beta)$ and $D(\alpha,\beta)$ takes the form $\lambda^2 - T(\alpha,\beta)\lambda + D(\alpha,\beta) = 0$. Hence, the two roots of this characteristic polynomial in terms of $T(\alpha,\beta)$ and $D(\alpha,\beta)$ are given by

$$\lambda_{1,2} = \frac{1}{2}T(\alpha,\beta) \pm \frac{1}{2}\sqrt{T^2(\alpha,\beta) - 4D(\alpha,\beta)}. \tag{3}$$

Expression (3) for the eigenvalues is studied through investigating the domain of T and D, which is the positive real cartesian plane $(\alpha,\beta) \in \mathbb{R}^2_+$. The classification that would cause the uniform steady state (u_s, v_s) to change stability and type due to the selection of the choice of the parameter values (α, β) is explored by examining the sign of the real part of eigenvalues [6,23,24,27]. For example the parameter space that makes the uniform steady state (u_s, v_s) stable, is the simultaneous combined choice of $\alpha, \beta \in \mathbb{R}_+$ that ensures the real part of the eigenvalues to be negative, which in turn is related to the discriminant of the roots expressed by (3). The full parameter space is investigated, so that all the possible types of influence due to the choice of parameters α and β on the stability and types of the uniform steady state (u_s, v_s) are encapsulated. The classification is conducted based on $\lambda_{1,2}$ to be a complex conjugate in the first case, then in the second case the parameter space is analysed when $\lambda_{1,2}$ are real roots. In each case, the space is further classified into stable and unstable regions.

2.1. Analysis for the case of complex eigenvalues

It is clear that the eigenvalues are a complex conjugate pair if and only if the discriminant is negative, which means the parameters (α, β) must satisfy the inequality

$$T^2(\alpha,\beta) - 4D(\alpha,\beta) = \gamma^2\left(\frac{\beta-\alpha-(\beta+\alpha)^3}{\beta+\alpha}\right)^2 - 4\gamma^2(\beta+\alpha)^2 < 0. \tag{4}$$

In order to find what region is satisfied by (4), we must find the critical curves on which the expression on the left of (4) is equal to zero, which means that the discriminant changes sign by moving across these curves in the plane $(\alpha,\beta) \in \mathbb{R}^2_+$. These curves can be found by solving the equation $T^2(\alpha,\beta) - 4D(\alpha,\beta) = 0$, which is true for the choice of $(\alpha,\beta) \in \mathbb{R}^2_+$, satisfying

$$\gamma^2\left(\frac{\beta-\alpha-(\beta+\alpha)^3}{\beta+\alpha}\right)^2 - 4\gamma^2(\beta+\alpha)^2 = 0. \tag{5}$$

The solution to (5) provides the boundaries, for the region of the plane that results in $\lambda_{1,2}$ to be a complex conjugate pair. The choice of (α, β) on the curves satisfying (5) enforces the eigenvalues of the system to be repeated real values, therefore, on these curves the steady state (u_s, v_s) becomes a star node, whose stability will be analysed in Section 2.2 for real eigenvalues. The left hand-side of (5) can be factorised in the form $\phi(\alpha, \beta)\psi(\alpha, \beta)$, which provides the equations of the two implicit curves $\phi(\alpha,\beta) = 0$ and $\psi(\alpha,\beta) = 0$, where ϕ and ψ are respectively given by

$$\begin{cases} \phi(\alpha,\beta) = \beta - \alpha - (\beta+\alpha)^3 - 2(\beta+\alpha)^2, \\ \psi(\alpha,\beta) = \beta - \alpha - (\beta+\alpha)^3 + 2(\beta+\alpha)^2. \end{cases} \tag{6}$$

Numerical solutions of (6) are simulated in Section 2.3. The solution of (6) alone serves to determine the boundaries of the complex region, without revealing which side of these implicit curves correspond to real eigenvalues and which side corresponds to complex eigenvalues. This can be decided, by finding another curve on which the eigenvalues are purely imaginary with zero real parts. Since the real part of the eigenvalues is given by $\frac{1}{2}T(\alpha,\beta)$ and the determinant $D(\alpha,\beta) = (\alpha+\beta)^2$ is strictly positive, therefore, the choice of (α, β) that solves the equation

$$T(\alpha,\beta) = 0 \quad \Longleftrightarrow \quad \frac{\beta-\alpha-(\beta+\alpha)^3}{\beta+\alpha} = 0, \tag{7}$$

will ensure that the eigenvalues of the system are purely imaginary. The curve satisfying Eq. (7) also forms the boundary for the positive and negative real parts of the eigenvalues $\lambda_{1,2}$ when they are complex conjugate pair, because on the curve satisfying (7) the real part of the eigenvalues are zero and hence changes the sign by moving across it. The numerical solutions of Eq. (7) are simulated in Section 2.3. It is worth noting that $T(\alpha,\beta) = 0$ is a sufficient condition for (u_s, v_s) to be a centre, due to the strictly positive expression for $D(\alpha,\beta) = (\alpha+\beta)^2$ in the discriminant. The real part

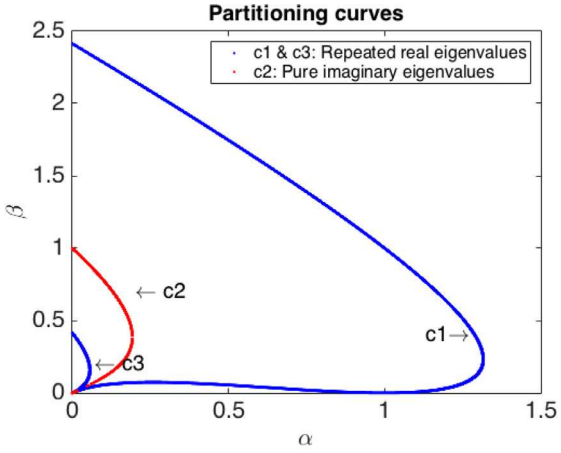

(a) The choice for α and β on curves $c1$ and $c3$ make (u_s, v_s) to be star node, whereas α and β on the curve $c2$ make (u_s, v_s) to be a centre with periodic oscillations.

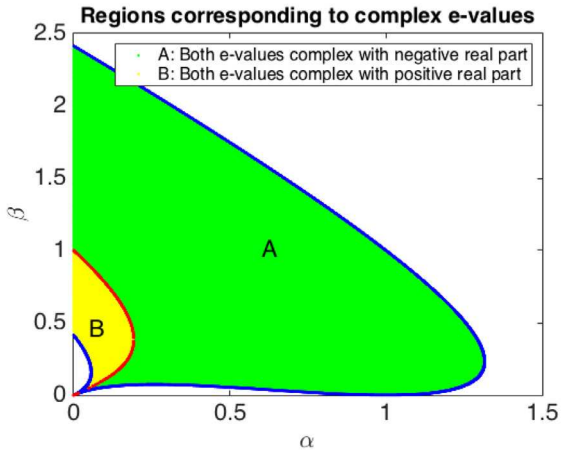

(b) The choice for α and β in the green region A results in (u_s, v_s) being a stable spiral, whereas α and β from the yellow region B results in (u_s, v_s) being an unstable spiral.

Fig. 1. Stable and unstable regions when the steady state (u_s, v_s) is a spiral stationary point.

of $\lambda_{1,2}$ is studied to find the stability classification of the parameter space, when $\lambda_{1,2}$ are complex conjugate pair. Knowing that the region bounded by $c1$ and $c3$ curves in Fig. 1 (a) results in $\lambda_{1,2}$ to be complex, the next step is to find which part of this region corresponds to positive real part of the complex numbers $\lambda_{1,2}$, and which part of this region corresponds to negative real part of $\lambda_{1,2}$. In order to determine their stability we must analyse the real part of $\lambda_{1,2}$, simultaneously with the assumption that the roots are a pair of complex conjugate numbers, which is given by

$$T(\alpha, \beta) = \frac{\beta - \alpha - (\beta + \alpha)^3}{\beta + \alpha}. \tag{8}$$

If the sign of (8) is negative in the region between the curves $c1$ and $c3$ in Fig. 1 (a), then (u_s, v_s) is a stable spiral, if it is positive then it is an unstable spiral. This means that the steady state (u_s, v_s) is a stable spiral if (α, β) simultaneously satisfy (4) and the inequality $\beta - \alpha < (\alpha + \beta)^3$ holds, which corresponds to the green region A shown in Fig. 1 (b). Similarly, the steady state (u_s, v_s) is an unstable spiral if parameters (α, β) simultaneously satisfy (4) and the inequality $\beta - \alpha > (\alpha + \beta)^3$, which is the yellow region B shown in Fig. 1 (b). It is worth noting that the trace $T(\alpha, \beta)$ for positive values of α and β is bounded by the value of 1 [see Section 4. Theorem 1], which means $\frac{\beta - \alpha - (\alpha+\beta)^3}{\beta+\alpha} \leq 1$ for all $\alpha, \beta \in \mathbb{R}_+$.

2.2. Analysis for the case of real eigenvalues

When both eigenvalues of the system are real numbers at the steady state (u_s, v_s) then the uniform steady state becomes a node. If $\lambda_{1,2}$ is a positive repeated root, then the steady state is an unstable star node. If $\lambda_{1,2}$ is a negative repeated root, then the steady state is a stable star node. Parameter space resulting in (u_s, v_s) to be a node can be analysed through studying the sign of $\lambda_{1,2}$, when both eigenvalues are real. This consequently means that the discriminant has to satisfy the inequality

$$T^2(\alpha, \beta) - 4D(\alpha, \beta) = \left(\frac{\beta - \alpha - (\beta + \alpha)^3}{\beta + \alpha}\right)^2 - 4(\beta + \alpha)^2 \geq 0. \tag{9}$$

Similarly, to the previous section, treating the equal case of (9) first will provide the boundaries between the real and complex regions for $\lambda_{1,2}$. These are $c1$ and $c3$ curves in Fig. 1 from the previous section. On $c1$ and $c3$ it was concluded that $\lambda_{1,2}$ are repeated real roots, which are precisely $\lambda_{1,2} = \frac{1}{2}\left(\frac{\beta - \alpha - (\beta+\alpha)^3}{\beta+\alpha}\right)$. In order to determine the stability of (u_s, v_s), when (α, β) are on $c1$ and $c3$ blue curves in Fig. 1, it is required to find the classification of this curve on which the sign of the repeated eigenvalue $\lambda_{1,2}$ is positive or negative. The steady state (u_s, v_s) is a star, if $\lambda_{1,2}$ is repeated real values, which means that the discriminant must be zero

$$T^2(\alpha, \beta) - 4D(\alpha, \beta) = \left(\frac{\beta - \alpha - (\beta + \alpha)^3}{\beta + \alpha}\right)^2 - 4(\beta + \alpha)^2 = 0. \tag{10}$$

The steady state (u_s, v_s) is a stable star if the choice of parameters (α, β) simultaneously satisfy (10) and the inequality $\beta - \alpha < (\alpha + \beta)^3$, which is the $c1$ curve in Fig. 2 (a) in blue colour. The steady state (u_s, v_s) is unstable star if the choice of parameters (α, β) simultaneously satisfy (10) and the inequality $\beta - \alpha > (\alpha + \beta)^3$, which is the $c3$ curve in Fig. 2 (a) in red colour.

The remaining region outside $c1$ and $c3$ curves in Fig. 2 (a) can be classified into two parts, one where (α, β) satisfies (9) and yet both $\lambda_{1,2}$ are distinct negative real values. This means that (α, β) must satisfy the inequality

$$\lambda_{1,2} = \frac{1}{2}\frac{\beta - \alpha - (\beta + \alpha)^3}{\beta + \alpha} \pm \sqrt{\left(\frac{\beta - \alpha - (\beta + \alpha)^3}{\beta + \alpha}\right)^2 - 4(\beta + \alpha)^2} < 0,$$

such that both eigenvalues are negative real. This is true if (α, β) satisfy the inequality

$$\frac{1}{2}\frac{\beta - \alpha - (\beta + \alpha)^3}{\beta + \alpha} + \sqrt{\left(\frac{\beta - \alpha - (\beta + \alpha)^3}{\beta + \alpha}\right)^2 - 4(\beta + \alpha)^2} < 0. \tag{11}$$

The region in the $(\alpha, \beta) \in \mathbb{R}_+$ plane satisfying (11) is denoted by A in Fig. 2 (b) shaded in green colour. The remaining region to analyse is the region outside the $c3$ curve in Fig. 2 (a). Any combination of (α, β) from this region corresponds to the remaining 2 cases, in which either one of λ_1 or λ_2 is positive, causing (u_s, v_s) to be a

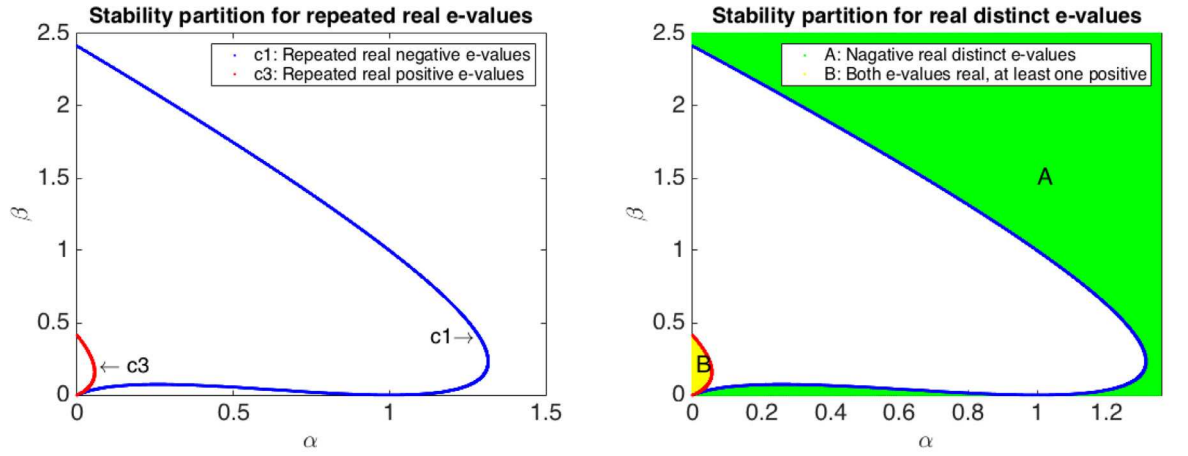

(a) The combination of (α, β) from $c1$, $c3$ (blue and red curves) results in (u_s, v_s) being an unstable star and a stable star respectively, which are both of type node.

(b) The combination of (α, β) from the yellow B and green A regions results in (u_s, v_s) being an unstable and a stable node respectively.

Fig. 2. Stable and unstable regions when the steady state (u_s, v_s) is a node.

saddle point which is unstable by definition. The other case is if $\lambda_{1,2}$ are both positive real values, which makes (u_s, v_s) to be an unstable node. The region satisfying the criteria for a saddle point or unstable node is indicated by B in Fig. 2 (b) in yellow colour. It is worth noting that the steady state (u_s, v_s) with either one or both positive real eigenvalues is by definition a saddle point or an unstable node, respectively. Under the current classification these both types fall under one category namely unstable node. The fact that one of the eigenvalues is real positive, hence as time grows very large, the behaviour of the solution is similar to that of an unstable node.

2.3. Numerical simulations in the absence of diffusion

A mesh is constructed on a square domain $D = [0, \alpha_{\max}] \times [0, \beta_{\max}]$, which is discretised by N points in both directions of α and β, where N is a positive integer. This provides a square mesh of $(N-1) \times (N-1)$ cells, each of size $\frac{\alpha_{\max}}{N} \times \frac{\beta_{\max}}{N}$, with N^2 points in D. To find the implicit numerical solution satisfying (6), at every mesh point in the direction α, the roots of the cubic polynomial in β namely $\phi(\alpha_i, \beta) = 0$, denoted by $\phi_i(\beta) = 0$ are computed using the Matlab command '*roots*'. It is worth noting that for every fixed α_i, one obtains $\phi_i(\beta)$, to be a cubic polynomial of degree three in β of the form

$$\phi_i(\beta) = C_0^i + C_1^i\beta + C_2^i\beta^2 + C_3^i\beta^3,$$

where the coefficients are given by $C_0^i = -\alpha_i - \alpha_i^3 - 2\alpha_i^2$, $C_1^i = 1 - 4\alpha_i - 3\alpha_i^2$, $C_2^i = -3\alpha_i - 2$, and $C_3^i = -1$. Similarly for each i in the direction of α, there are N cubic polynomials in β satisfying $\psi_i(\beta) = 0$, with ψ_i of the form

$$\psi_i(\beta) = C_0^i + C_1^i\beta + C_2^i\beta^2 + C_3^i\beta^3,$$

where $C_0^i = -\alpha_i - \alpha_i^3 + 2\alpha_i^2$, $C_1^i = 1 + 4\alpha_i - 3\alpha_i^2$, $C_2^i = -3\alpha_i + 2$, and $C_3^i = -1$. Using similar notation, it can be shown that solving (7) is equivalent to finding the set of $(\alpha, \beta) \in \mathbb{R}_+^2$ such that the equation $h(\alpha, \beta) = 0$ satisfying (7) is true, where for every $i = 1, \ldots, N$ a polynomial of degree three in β denoted by $h_i(\beta)$ is given by

$$h_i(\beta) = C_0^i + C_2^i\beta + C_2^i\beta^2 + C_3^i\beta^3,$$

with coefficients $C_0^i = -\alpha_i - \alpha_i^3$, $C_1^i = 1 - \alpha_i^2$, $C_2^i = -3\alpha_i$, and $C_3^i = -1$. Each of the equations $\phi_i(\beta) = 0$, $\psi_i(\beta) = 0$ and $h_i(\beta) = 0$ have at most three distinct roots namely $(\beta_1, \beta_2, \beta_3)$ for every fixed α_i, which means for every fixed α_i the three points namely (α_i, β_j) for $j = 1, 2, 3$ are the three points that lie on the implicit curves given by (6) and (7). Since (α, β) are positive real parameters in the system, therefore, at every fixed α_i, only the positive real roots β_j are considered and any root that is either real negative or complex is ignored. Fig. 1, was simulated for $\alpha_{\max} = \beta_{\max} = 5$ and $N = 5000$, which means the curves $c1$, $c2$ and $c3$ are respectively formed from the positive real roots of 5000 cubic polynomials, namely $\psi_i(\beta) = 0$, $h_i(\beta) = 0$ and $\phi_i(\beta) = 0$ for $i = 1, \ldots, 5000$. The curves $c1$ and $c3$ in Fig. 1 (a) are the critical boundaries, at which the type of the steady state (u_s, v_s) changes from node to a spiral or vice versa, depending on whether one enters or exists the region between $c1$ and $c3$. The positive real combination of (α, β) that satisfies (7) corresponding to $h_i(\beta) = 0$ is given by the red $c2$ curve in Fig. 1 (a). The location of $c2$ curve also indicates that the region between the curves $c1$ and $c3$ results in that $\lambda_{1,2}$ are complex numbers. If (α, β) are chosen from values on curves $c1$ and $c3$, then the eigenvalues will be repeated real roots, since on these curves the discriminant is zero. However if (α, β) are chosen from the values on the curve $c2$ then the eigenvalues are purely imaginary of the form $\lambda_{1,2} = \pm i\sqrt{4D(\alpha, \beta)} = \pm i2(\alpha + \beta)$. This implies that the steady state (u_s, v_s) is a centre with the system exhibiting periodic oscillations around the uniform steady state.

The numerical package for ordinary differential equations *ode45* in MATLAB was employed to simulate and visualise the local behaviour of the system (2) near the uniform steady state (u_s, v_s). Each simulation was run up to a final time $T = 5$, starting at the initial time $T = 0$, with time step $\tau = 5 \times 10^{-2}$. Parameter values were chosen from the regions A, B and on the curve $c2$ from Fig. 1 (b) and (a) respectively, which are then plotted with 8 trajectories around the uniform steady state (u_s, v_s). Fig. 3 shows that the behaviour of the trajectories around the uniform steady state in each case is in agreement with the theoretically predicted type of (u_s, v_s). The summary of the chosen numerical values for these simulations are all summarised in Table 1 and these are also indicated in the relevant captions for each figure. The eigenvalues of the stability matrix for each choice of the parameters and at

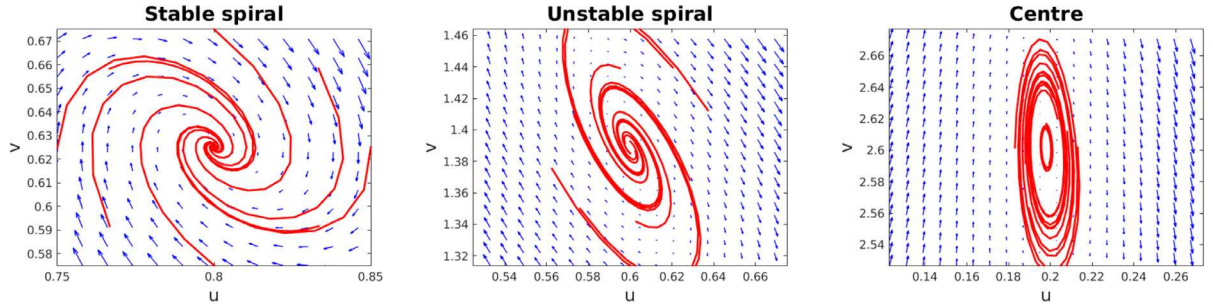

(a) Parameters $(\alpha, \beta) = (0.4, 0.4)$, resulting in the uniform steady state $(u_s, v_s) = (0.8, 0.625)$ and eigenvalues $\lambda_{1,2} = -0.32 \pm 0.73i$.

(b) Parameters $(\alpha, \beta) = (0.1, 0.5)$, resulting in the uniform steady state $(u_s, v_s) = (0.6, 1.39)$ and eigenvalues $\lambda_{1,2} = 0.15 \pm 0.58i$.

(c) Parameters $(\alpha, \beta) = (0.096, 0.102)$, resulting in the uniform steady state $(u_s, v_s) = (0.198, 2.6)$ and eigenvalues $\lambda_{1,2} = \pm 0.20i$.

Fig. 3. Phase-plane diagrams of the model system in the absence of diffusion for types of steady states with complex $\lambda_{1,2}$, computed correct up to 2 decimal places and $i = \sqrt{-1}$.

Table 1
Table showing the summary of all types of steady states and their corresponding phase-plane diagrams with reference to the parameter space on $(\alpha, \beta) \in \mathbb{R}_+$ plane.

Name (SS)	(α, β)	(u_s, v_s)	$\lambda_{1,2}$	Fig 5(a)	Phase-plane
Stable node	(1.400, 2.000)	(3.400, 0.173)	(−10.26, −1.13)	Region A	Fig 4 (a)
Unstable node	(0.020, 0.130)	(0.150, 5.780)	(0.03, 0.68)	Region B	Fig 4 (b)
Stable spiral	(0.400, 0.400)	(0.800, 0.625)	$-0.32 \pm 0.73i$	Region C	Fig 3 (a)
Unstable spiral	(0.100, 0.500)	(0.600, 1.390)	$0.15 \pm 0.58i$	Region D	Fig 3 (b)
Stable star	(0.400, 0.066)	(0.470, 0.310)	(−0.47, −0.47)	Curve $c1$	Fig 4 (c)
Unstable star	(0.060, 0.180)	(0.230, 3.250)	(0.20, 0.20)	Curve $c3$	Fig 4 (d)
Centre	(0.096, 0.102)	(0.198, 2.600)	$\pm 0.20i$	Curve $c2$	Fig 3 (c)

the corresponding uniform steady state are presented in the corresponding captions. In each simulation the vertical axes correspond to the variable v and the horizontal axes correspond to the variable u. The red trajectories show the interactive behaviour of u and v in relation to the corresponding steady state.

The physical interpretation of this classification is that, whenever the choice of α and β is taken from region B in Fig. 1 then the dynamics of the perturbed system near the constant steady state (u_s, v_s) will spirally move away as time grows, which resembles the shape of an outward spreading spiral. This behaviour is shown in Fig. 3 (b). However if the parameter values are chosen from region A, then the dynamics of the perturbed system will spirally move in towards the constant stable steady state (u_s, v_s), therefore, any trajectory near the steady state forms the shape of spiral that is uniformly moving towards its centre, which is the constant steady state namely the point (u_s, v_s). This behaviour is shown in Fig. 3 (a). If the values of the parameters are chosen from those on the curve c_2, then the dynamics of the system behaves in such a way that it neither goes away from the steady state, and nor does it reach the steady state, instead the trajectories of the system move on fixed orbits around the uniform steady state (u_s, v_s), forming either circles or ellipse. This behaviour of u and v is shown in Fig. 3 (c).

System (2) is also numerically simulated using *ode45* package in MATLAB to visualise the behaviour of trajectories in the neighbourhood of (u_s, v_s), when $\lambda_{1,2}$ are real values. Each simulation is tested on the phase plane diagram to observe the trajectories of solution. In each case the steady state (u_s, v_s) is computed and eight trajectories around the steady state whose behaviour is governed by the relevant vector-field plotted as blue arrows.

If parameters are selected from the curve c_1 in Fig. 2 (b), then the eigenvalues are positive real repeated roots. The dynamics of the perturbed system near the constant steady steady state will radially move outward (see Fig. 4 (d)). If the values of α and β are chosen from those lying on the c_3 curve in Fig. 2 (b), then the local dynamics of the system near the constant steady state radially move inward towards the point (u_s, v_s) (see Fig. 4 (c)). Similarly, if α and β are chosen from region A in Fig. 2 (b), it will result in $\lambda_{1,2}$ to be a pair of distinct negative real roots. This means for the dynamics of the system to move towards the stable constant steady state. If parameters are however chosen from region B in Fig. 2 (b), this results in the constant steady state to be an unstable node, it means the behaviour of trajectories near the steady state are expected to behaviour similarly to those corresponding to the curve $c3$ (see Fig. 4 (a)).

In general, the parameter space that influences the nature of the uniform steady state (u_s, v_s) can be categorised into four different regions, which are separated by three curves. This classification is in principle equivalent to that presented in [23], however the distinction with the current work is that for the specific system given by (2) the full parameter plane is classified subject to the proposed theory given in [23]. Each region is characterised and the behavior of the uniform steady state is established by choosing parameters α and β from the region. Fig. 5 (a) summarises the full classification of the parameter space in the absence of diffusion for the uniform steady state (u_s, v_s). It can be noted that in terms of stability only and irrespective of the type of the steady state, the full parameter space namely the $(\alpha, \beta) \in \mathbb{R}_+$ plane can be classified into two regions namely stable or unstable, this is the partition established by the location of the yellow curve in Fig. 5 (a). Stability classification irrespective of the type of steady state is ex-

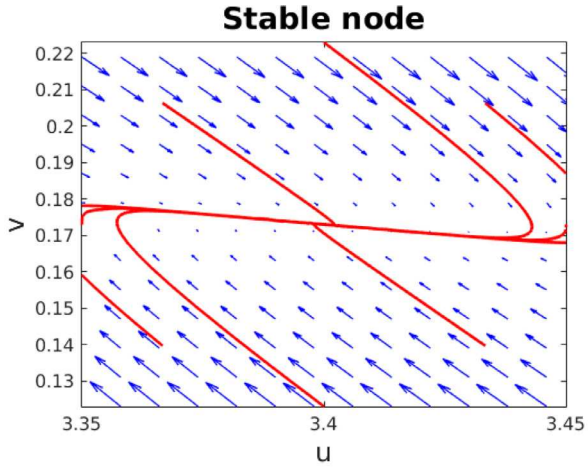

(a) Parameters $(\alpha, \beta) = (1.4, 2.0)$, resulting in the uniform steady state $(u_s, v_s) = (3.4, 0.173)$ and eigenvalues $\lambda_{1,2} = (-10.26, -1.13)$.

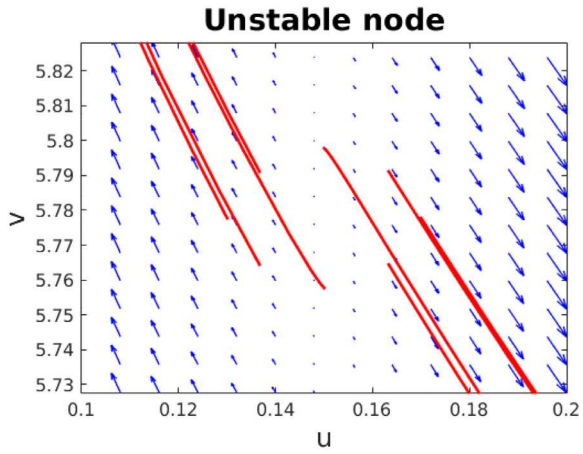

(b) Parameters $(\alpha, \beta) = (0.02, 0.13)$, resulting in the uniform steady state $(u_s, v_s) = (0.15, 5.78)$ and eigenvalues $\lambda_{1,2} = (0.03, 0.68)$.

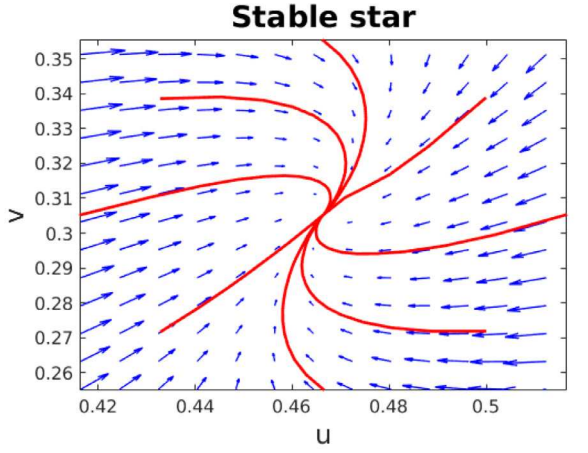

(c) Parameters $(\alpha, \beta) = (0.40, 0.066)$, resulting in the uniform steady state $(u_s, v_s) = (0.8, 0.625)$ and eigenvalues $\lambda_{1,2} = (-0.47, -0.47)$.

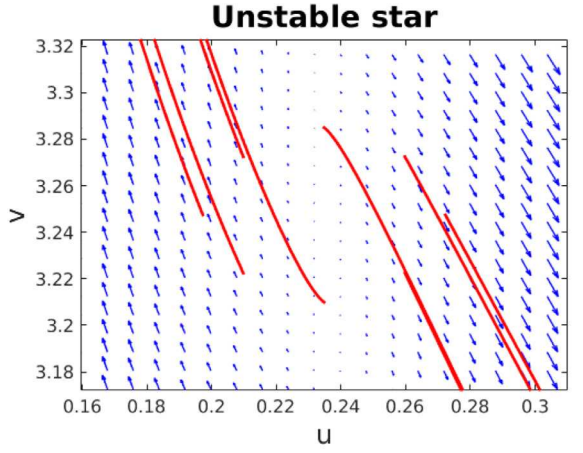

(d) Parameters $(\alpha, \beta) = (0.06, 0.18)$, resulting in the uniform steady state $(u_s, v_s) = (0.23, 3.25)$ and eigenvalues $\lambda_{1,2} = (0.20, 0.20)$.

Fig. 4. Phase-plane diagrams of the model system in the absence of diffusion characterising the stability of the steady states for real $\lambda_{1,2}$.

plicitly presented in Fig. 5 (b). The purpose of stability partition will prove beneficial in the next section when the diffusion-driven instability is explored. Because diffusion-driven instability as the name suggests, is to explore how a stable steady state becomes unstable for the same choice of parameters (α, β), when diffusion is added to the system. Therefore, with the help of stability partition, one is able to observe the change in the location of the yellow curve in Fig. 5 (b). Table 1 shows the values of the parameters (α, β) and the values of the unique steady state (u_s, v_s) with the relative eigenvalues that correspond to the summary of the full classification of parameter space presented in Fig. 5 (a), and these parameter values are used in the numerical simulations.

3. Stability analysis in the presence of diffusion

It is intuitive to understand that normally diffusion serves to enhance spatial homogeneity of concentration gradients [23,36], however, in the case of reaction-diffusion systems, it has the opposite effect in that the uniform steady state which was stable in the absence of diffusion becomes unstable in its presence [23,35,36,39]. In this work, the mathematical rigor of how reaction and diffusion together can give rise to instability is investigated, which is responsible for diffusion-driven pattern formation. One of the explicit aims of the current work is to investigate the consequences of the conditions of diffusion-driven instability on the classification of the parameter space in the presence of diffusion. Furthermore, we want to explore quantitative relationship between the domain size and the types of diffusion-driven instability.

The uniform steady state (u_s, v_s) as previously mentioned satisfies the system with diffusion (1) and the zero-flux boundary conditions, therefore, without loss of generality, (u_s, v_s) is considered a steady state of the system in presence of diffusion as well. System (1) is first linearised by introducing new variables namely $\bar{u}$ and $\bar{v}$ in such a way that they are perturbed slightly from the

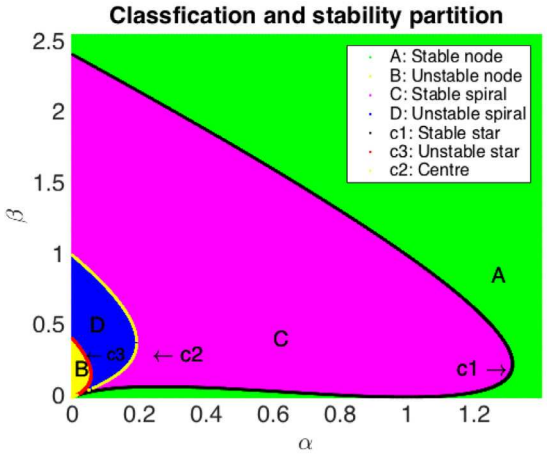

(a) Parameter space classification that results in the steady state (u_s, v_s) to be of different types, and their corresponding stability as indicated in the legend.

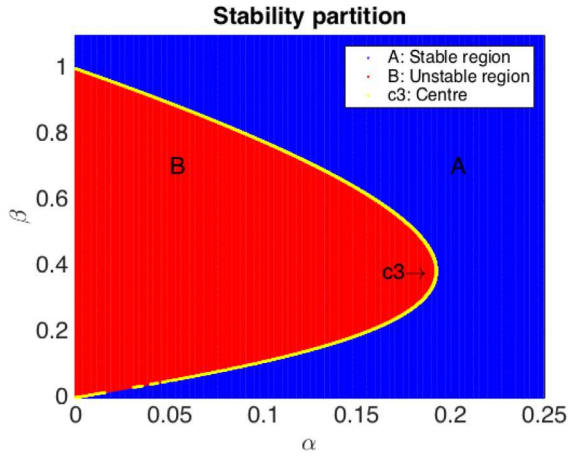

(b) Parameters from red region make (u_s, v_s) unstable, whereas any combination of (α, β) from the blue region make (u_s, v_s) stable, and parameters lying on the yellow curve results in (u_s, v_s) being a centre.

Fig. 5. The full parameter classification for the stability and types of the steady state (u_s, v_s).

steady state (u_s, v_s), so that their relationships to u and v are $(\bar{u}, \bar{v}) = (u - u_s, v - v_s)$. For u and v, the perturbed variables $\bar{u} + u_s$ and $\bar{v} + v_s$ are substituted in (1) and expanded using Taylor expansion for functions of two variables to obtain a linearised system which can be written in matrix form as

$$\frac{\partial}{\partial t}\begin{bmatrix}\bar{u}\\ \bar{v}\end{bmatrix} = \begin{bmatrix}1 & 0\\ 0 & d\end{bmatrix}\begin{bmatrix}\triangle\bar{u}\\ \triangle\bar{v}\end{bmatrix} + \begin{bmatrix}\frac{\partial f}{\partial u}(u_s, v_s) & \frac{\partial f}{\partial v}(u_s, v_s)\\ \frac{\partial g}{\partial u}(u_s, v_s) & \frac{\partial g}{\partial u}(u_s, v_s)\end{bmatrix}\begin{bmatrix}\bar{u}\\ \bar{v}\end{bmatrix}. \tag{12}$$

In order to complete the linearisation in the presence of diffusion, it is necessary to find the eigenfunctions of the Laplace operator, that satisfies the homogeneous Neumann boundary conditions. Eigenfunctions of the Laplace operator on planar domains are well-studied in the literature [6,8,24,39]. It is presumed that $\bar{u}$ and $\bar{v}$ both are of a similar form. The eigenfunctions for the Laplace operator are found by solving the relevant eigenvalue problems, that satisfy the given boundary conditions of problem (1). Such an eigenvalue problem is of the form

$$\begin{cases}\dfrac{\partial^2\bar{u}}{\partial x^2} + \dfrac{\partial^2\bar{u}}{\partial y^2} = \eta\bar{u}, & \eta \in \mathbb{R},\\ \dfrac{\partial\bar{u}}{\partial x}(0, y) = 0, & \dfrac{\partial\bar{u}}{\partial x}(L, y) = 0, \quad 0 \le y \le L,\\ \dfrac{\partial\bar{u}}{\partial y}(x, 0) = 0, & \dfrac{\partial\bar{u}}{\partial y}(x, L) = 0, \quad 0 \le x \le L.\end{cases} \tag{13}$$

The method of separation of variables is used to find the solution to problem (13) by presuming that the solution is in the form of a product of two functions namely $X(x)$ and $Y(y)$, so $\bar{u}$ has the form $\bar{u}(x, y) = X(x)Y(y)$. This form of solution is substituted in equation (13) to obtain two one-dimensional eigenvalue problems, which are individually solved and the resulting set of eigenfunctions solving (13) are given by $\bar{u}_{n,m}(x, y) = C_{n,m}\cos\left(\frac{n\pi x}{L}\right)\cos\left(\frac{m\pi y}{L}\right)$, where $C_{n,m}$ are the coefficients depending on the mode of the eigenfunctions. The solution to problem (12) can be, therefore, written as the sum of infinite expansion in the form of the product of $T(t)$, and the eigenfunctions for the two dimensional Laplace operator, so we have

$$\bar{u}(x, y, t) = \sum_{n=0}^{\infty}\sum_{m=0}^{\infty} U_{n,m}\exp(\lambda_{n,m}t)\cos\left(\frac{n\pi x}{L}\right)\cos\left(\frac{m\pi y}{L}\right),$$

$$\bar{v}(x, y, t) = \sum_{n=0}^{\infty}\sum_{m=0}^{\infty} V_{n,m}\exp(\lambda_{n,m}t)\cos\left(\frac{n\pi x}{L}\right)\cos\left(\frac{m\pi y}{L}\right),$$

where $U_{n,m}$ and $V_{n,m}$ are the coefficients of the infinite expansion. Substituting this form of solution in (12), the problem can be written as a two-dimensional discrete set of algebraic equations in the form, with $\lambda = \lambda_{n,m}$

$$\lambda\begin{bmatrix}\bar{u}\\ \bar{v}\end{bmatrix} = -\frac{(n^2+m^2)\pi^2}{L^2}\begin{bmatrix}1 & 0\\ 0 & d\end{bmatrix}\begin{bmatrix}\bar{u}\\ \bar{v}\end{bmatrix} + \gamma\begin{bmatrix}\frac{\beta-\alpha}{\beta+\alpha} & (\beta+\alpha)^2\\ -\frac{2\beta}{\beta+\alpha} & -(\beta+\alpha)^2\end{bmatrix}\begin{bmatrix}\bar{u}\\ \bar{v}\end{bmatrix}, \tag{14}$$

which can also be written as a two-dimensional discrete eigenvalue problem

$$\begin{bmatrix}\gamma\frac{\beta-\alpha}{\beta+\alpha} - \frac{(n^2+m^2)\pi^2}{L^2} & \gamma(\beta+\alpha)^2\\ -\gamma\frac{2\beta}{\beta+\alpha} & -\gamma(\beta+\alpha)^2 - d\frac{(n^2+m^2)\pi^2}{L^2}\end{bmatrix}\begin{bmatrix}\bar{u}\\ \bar{v}\end{bmatrix} = \lambda\begin{bmatrix}\bar{u}\\ \bar{v}\end{bmatrix}. \tag{15}$$

For the stability of the steady state (u_s, v_s) in the presence of diffusion, the eigenvalues of problem (15) are analysed. The characteristic polynomial for (15) is given by

$$\begin{vmatrix}\gamma\frac{\beta-\alpha}{\beta+\alpha} - \frac{(n^2+m^2)\pi^2}{L^2} - \lambda & \gamma(\beta+\alpha)^2\\ -\gamma\frac{2\beta}{\beta+\alpha} & -\gamma(\beta+\alpha)^2 - d\frac{(n^2+m^2)\pi^2}{L^2} - \lambda\end{vmatrix} = 0, \tag{16}$$

which is a quadratic polynomial in λ. Let $\mathcal{T}$ and $\mathcal{D}$ denote the trace and determinant of the stability matrix (15) then the pair of eigenvalues $\lambda_{1,2}$ of system (15) satisfy the quadratic polynomial in terms of the trace and determinant in the form

$$\lambda^2 - \mathcal{T}(\alpha, \beta)\lambda + \mathcal{D}(\alpha, \beta) = 0, \tag{17}$$

where $\mathcal{T}(\alpha,\beta)$ and $\mathcal{D}(\alpha,\beta)$ are given by

$$\mathcal{T}(\alpha,\beta) = \gamma\frac{\beta-\alpha-(\beta+\alpha)^3}{\beta+\alpha} - (d+1)\frac{(n^2+m^2)\pi^2}{L^2},$$

$$\mathcal{D}(\alpha,\beta) = \left(\gamma\frac{\beta-\alpha}{\beta+\alpha} - \frac{(n^2+m^2)\pi^2}{L^2}\right) \times\left(-\gamma(\beta+\alpha)^2 - (d+1)\frac{(n^2+m^2)\pi^2}{L^2}\right) +2\gamma^2\beta(\beta+\alpha).$$

The roots of (17) are $\lambda_{1,2} = \frac{1}{2}\mathcal{T}(\alpha,\beta) \pm \frac{1}{2}\sqrt{\mathcal{T}^2(\alpha,\beta) - 4\mathcal{D}(\alpha,\beta)}$. We note that, in comparison to the case when no diffusion is present, the trace $\mathcal{T}(\alpha,\beta)$ of the Jacobian matrix becomes more negative when diffusion is introduced since a positive quantity is being subtracted, thereby enhancing the stability of the system. This is equivalent to the default intuition that diffusion may only promote stability, due to its natural property of homogenising concentration gradient. However, the modification to the determinant part $\mathcal{D}(\alpha,\beta)$ in the form of an additional positive term $(d+1)\pi^4\frac{(n^2+m^2)^2}{L^4}$ is intuitively expected to dominate the strictly positive term which is subtracted from $\mathcal{T}(\alpha,\beta)$, namely $(d+1)\frac{(n^2+m^2)\pi^2}{L^2}$. These modifications to the trace and the determinant of the stability matrix due to the presence of diffusion to the system are investigated thoroughly to derive possible quantitative relationships between domain size, reaction and diffusion rates in the context of the parameter classification. We also attempt to quantitatively understand how this modification of both $\mathcal{T}(\alpha,\beta)$ and $\mathcal{D}(\alpha,\beta)$ contributes to creating instability. The regions of the parameter space for all types of steady states and their stability is analysed. Once the regions for different types of steady states are classified, then subject to this classification the influence of the domain size Ω is explored on the types and existence of diffusion-driven instabilities. To determine the types of steady state (u_s, v_s), with corresponding parameter space, it is important to realise that despite the dependence on α and β, the type of steady state also depends on the additional parameters namely γ, d and L. The variation of the additional parameters are investigated for fixed n and m to explore how the parameter space varies for different values of d, for example. Another important relationship to investigate is between the area of the domain L^2 and the reaction rate γ and how these influence the process of diffusion-driven instability.

3.1. Analysis for the case of complex eigenvalues

The eigenvalues $\lambda_{1,2}$ are complex values if $(\alpha,\ \beta)$ are chosen such that the discriminant of (17) is negative. It means that $(\alpha,\ \beta)$ must satisfy

$$\frac{1}{4}\mathcal{T}^2(\alpha,\beta) < \mathcal{D}(\alpha,\beta). \tag{18}$$

One immediate consequence of this inequality is that $\mathcal{D}(\alpha,\beta)$ must be positive, because if $\mathcal{D}(\alpha,\beta)$ is negative, then for no choice of $(\alpha,\ \beta)$ do the eigenvalues $\lambda_{1,2}$ become complex. This immediate observation is automatically in agreement with the conditions for diffusion-driven instability presented in [6,20,24]. Furthermore, this condition on one hand will determine the region of the $(\alpha,\beta)\in\mathbb{R}_+$ plane on which $\lambda_{1,2}$ are a complex conjugate pair. On the other hand it serves to indicate the equations for the partitioning implicit curves on which the eigenvalues change type from real to complex. Bearing in mind, that inequality (18) is a sufficient condition for $\lambda_{1,2}$ to have imaginary parts, therefore, it suffices to study (18) for $(u_s,\ v_s)$ to be a spiral. Before numerical treatment of the critical curve for the complex region, the stability of $(u_s,\ v_s)$ is studied analytically given that $\lambda_{1,2}$ have imaginary parts. Stability of $(u_s,\ v_s)$ is determined by the sign of the real part of $\lambda_{1,2}$ when it is a pair of complex conjugate values. Given that this is the case then the real part of $\lambda_{1,2}$ is given by

$$\mathrm{Re}(\lambda_{1,2}) = \frac{1}{2}\left(\gamma\frac{\beta-\alpha-(\beta+\alpha)^3}{\beta+\alpha} - (d+1)\frac{(n^2+m^2)\pi^2}{L^2}\right).$$

If we wish to find the parameter space for which $(u_s,\ v_s)$ is temporally unstable then we require the real part of both eigenvalues to be positive, which means in addition to the condition (18) we want $\mathcal{T}(\alpha,\beta)$ to be positive or equivalently $(\alpha,\ \beta)$ must satisfy

$$\gamma\frac{\beta-\alpha-(\beta+\alpha)^3}{\beta+\alpha} > (d+1)\frac{(n^2+m^2)\pi^2}{L^2}. \tag{19}$$

This relationship indicates that the stability of $(u_s,\ v_s)$ when $\lambda_{1,2}$ are complex, depends on the extra parameters L, d and γ. The maximum of the left-hand side of (19) is the non-zero positive constant γ [see Section 4, Theorem 1], which suggests the real part of $\lambda_{1,2}$ becomes positive if the parameter L satisfies

$$L^2 > \pi^2\frac{(d+1)(m^2+n^2)}{\gamma}. \tag{20}$$

This claim is formally proven in Theorem 1. In the absence of diffusion, in the region where $(u_s,\ v_s)$ is a spiral, there are sub-regions that correspond to a stable spiral as well as sub-regions that correspond to an unstable spiral. One immediate consequence of including diffusion, into the model, is that it puts the condition (23) on the domain size L^2 for the real part of $\lambda_{1,2}$ to be positive. If the real part of the complex eigenvalues becomes zero, then the roots become purely imaginary, indicating that the system undergoes a time-periodic oscillations whilst experiencing spatial stability. This type of instability is referred to as *Transcritical bifurcation* and this entails that the real part of $\lambda_{1,2}$ must become zero, which means

$$\gamma\frac{\beta-\alpha-(\beta+\alpha)^3}{\beta+\alpha} - (d+1)\frac{(n^2+m^2)\pi^2}{L^2} = 0. \tag{21}$$

Rearranging (21) and solving for L^2, the necessary condition for transcritical bifurcation is obtained in the form

$$L^2 = \frac{(\beta+\alpha)(d+1)(n^2+m^2)\pi^2}{\gamma\left(\beta-\alpha-(\alpha+\beta)^3\right)}. \tag{22}$$

If the parameter L satisfies condition (23) simultaneously with condition (22) and $\mathcal{D}(\alpha,\beta) > 0$, then the system exhibits a transcritical bifurcation. However, if condition (22) is relaxed and yet parameters L, γ and d are given to satisfy condition (23) then the dynamics of the system exhibit temporally periodic behaviour. Upon increasing the value of d, yet maintaining condition (23) the system is expected to become temporally unstable. This type of instability is referred to as *Hopf Bifurcation*, where adding diffusion to a temporally stable system, causes temporal instability. The results of the analysis of the case with complex eigenvalues are formally stated and proven in the following theorem.

Theorem 1 (Hopf or transcritical bifurcation)**.** *Let u and v satisfy the non-dimensional reaction-diffusion system with* activator-depleted *reaction kinetics (1) on a square domain $\Omega\subset\mathbb{R}^2$ with length L and positive parameters γ, $d > 0$, $\alpha > 0$ and $\beta > 0$. For the system to exhibit Hopf or transcritical bifurcation in the neighbourhood of the unique steady state $(u_s, v_s) = \left(\alpha+\beta, \frac{\beta}{(\alpha+\beta)^2}\right)$, the necessary condition on the area L^2 of the square domain $\Omega\subset\mathbb{R}^2$ is*

$$L^2 \geq \pi^2\frac{(d+1)(m^2+n^2)}{\gamma}, \tag{23}$$

where m and n are any integers.

Proof. The important step in this proof is to derive under what condition on L is the expression for $\mathcal{T}(\alpha,\beta)$ guaranteed to be positive, because when $\lambda_{1,2}$ are complex eigenvalues then the sign of

$\mathcal{T}(\alpha,\beta)$ is precisely what determines the stability of (u_s, v_s). The system undergoes Hopf or transcritical bifurcation in the neighbourhood of (u_s, v_s), if the sign $\mathcal{T}(\alpha,\beta)$ is positive. Therefore for diffusion-driven instability to influence (u_s, v_s) when $\lambda_{1,2}$ are complex conjugate pair it is necessary that

$$\mathcal{T}(\alpha,\beta)=\gamma\frac{\beta-\alpha-(\beta+\alpha)^3}{\beta+\alpha}-(d+1)\frac{(n^2+m^2)\pi^2}{L^2}\geq 0, \tag{24}$$

which can equivalently be written as

$$\gamma\frac{\beta-\alpha-(\beta+\alpha)^3}{\beta+\alpha}\geq(d+1)\frac{(n^2+m^2)\pi^2}{L^2}. \tag{25}$$

The expression on the left hand-side of (25) is explored in particular to find its upper bound, it can be written it in the form of difference between two rational functions as

$$\gamma\frac{\beta-\alpha-(\beta+\alpha)^3}{\beta+\alpha}=\gamma\Big(f_1(\alpha,\beta)-f_2(\alpha,\beta)\Big), \tag{26}$$

where $f_1(\alpha,\beta)=\frac{\beta}{\beta+\alpha}$ and $f_2(\alpha,\beta)=\frac{\alpha+(\beta+\alpha)^3}{\beta+\alpha}$. The range for $f_1(\alpha,\beta)$ and $f_2(\alpha,\beta)$ are independently analysed to find the supremum of the expression on the left of (26). Starting with $f_1(\alpha,\beta)$, which is bounded below and above in the domain $(\alpha,\beta)\in[0,\infty)\times[0,\infty)$, we have $\sup_{\alpha,\beta\in\mathbb{R}_+} f_1(\alpha,\beta)=1$, and the $\inf_{\alpha,\beta\in\mathbb{R}_+} f_1(\alpha,\beta)=0$ for all $\alpha,\beta\in\mathbb{R}_+$. Similarly considering the expression for $f_2(\alpha,\beta)$, we have $\sup_{\alpha,\beta\in\mathbb{R}_+} f_2(\alpha,\beta)=\infty$, and the $\inf_{\alpha,\beta\in\mathbb{R}_+} f_2(\alpha,\beta)=0$, for all $\alpha,\beta\in\mathbb{R}_+$. Since the ranges of both $f_1(\alpha,\beta)$ and $f_2(\alpha,\beta)$ are non-negative within their respective domains, therefore the supremum of their difference is determined by the supremum of the function with positive sign, which is $\sup_{\alpha,\beta\in\mathbb{R}_+} f_1(\alpha,\beta)=1$. Therefore, inequality (24) can be written as

$$\begin{aligned}(d+1)\frac{(n^2+m^2)\pi^2}{L^2}&\leq\gamma\frac{\beta-\alpha-(\beta+\alpha)^3}{\beta+\alpha}\\&\leq\gamma\sup_{\alpha,\beta\in\mathbb{R}_+}\Big(f_1(\alpha,\beta)-f_2(\alpha,\beta)\Big)\\&=\gamma\sup_{\alpha,\beta\in\mathbb{R}_+}f_1(\alpha,\beta)=\gamma,\end{aligned}$$

which by rearranging leads to the desired condition (23). □

3.2. Analysis for the case of real eigenvalues

The eigenvalues $\lambda_{1,2}$ are both real if the discriminant of the roots is either zero or positive, which in turn means that both eigenvalues are real values if the relationship between $\mathcal{T}(\alpha,\beta)$ and $\mathcal{D}(\alpha,\beta)$ is such that

$$\mathcal{T}^2(\alpha,\beta)\geq 4\mathcal{D}(\alpha,\beta). \tag{27}$$

The equal case of (27) is looked at first, where we have

$$\mathcal{T}^2(\alpha,\beta)=4\mathcal{D}(\alpha,\beta), \tag{28}$$

which means that the discriminant is zero, hence the roots are repeated real values of the form $\lambda_1=\lambda_2\in\mathbb{R}$, given by

$$\lambda_1=\lambda_2=\frac{1}{2}\Big(\gamma\frac{\beta-\alpha-(\beta+\alpha)^3}{\beta+\alpha}-(d+1)\frac{(n^2+m^2)\pi^2}{L^2}\Big). \tag{29}$$

When α and β satisfy condition (28), the stability of the steady state is determined by the sign of the root itself. The expression given by (29) can be easily shown to be negative if the area L^2 of the domain satisfies the inequality

$$L^2<\pi^2\frac{(\beta+\alpha)(d+1)(n^2+m^2)}{\gamma\big(\beta-\alpha-(\beta+\alpha)^3\big)}. \tag{30}$$

Otherwise, the repeated root is positive provided that L satisfies

$$L^2>\pi^2\frac{(\beta+\alpha)(d+1)(n^2+m^2)}{\gamma\big(\beta-\alpha-(\beta+\alpha)^3\big)}. \tag{31}$$

Analysing (30) and (31) carefully, it can be observed that the only terms that can possibly invalidate the inequalities are in the denominator of the right hand-side, namely the expression $\beta-\alpha-(\beta+\alpha)^3$. Therefore, a restriction is required to be stated on this term to ensure that the area of Ω is not compared against a negative quantity, such a restriction is

$$\beta>\alpha+(\beta+\alpha)^3. \tag{32}$$

It must be noted that (32) is the same restriction on the parameter choice obtained for the case of repeated real eigenvalues in the absence of diffusion. The region where the eigenvalues are real repeated roots are implicit curves in the parameter space satisfying (28), these curves are computed numerically in Section 3.3. These curves form the boundary between the regions of complex and real eigenvalues. Varying the diffusion rate d causes a shift to the location of the curves indicating clearly regions that are subject to diffusion-driven instability. The remaining case to look at is when both eigenvalues are real distinct. This happens if α and β are chosen such that the strict inequality case of (27) is satisfied. This case corresponds to the diffusion-driven instability *Turing type* only, because both eigenvalues are real and distinct.

The role of the domain-size is studied to analyse its importance in temporal stability, which requires the real part of $\lambda_{1,2}$ to be negative in all cases when $\lambda_{1,2}\in\mathbb{C}\backslash\mathbb{R}$ and suggests that the term on the right-hand side of (19) satisfies

$$(d+1)\frac{(n^2+m^2)\pi^2}{L^2}>\gamma\quad\Longleftrightarrow\quad L^2<\pi^2\frac{(d+1)(m^2+n^2)}{\gamma}. \tag{33}$$

If the diffusion rate d is increased, yet satisfying (34), instability is still expected to invade stable regions in the parameter plane, however the only type of instability one may expect is spatial and not temporal. This type of instability is referred to as *Turing Instability* [2,23,36], where a certain region in the parameter space is stable in the absence of diffusion and yet becomes spatially unstable upon adding diffusion to the system. For the first eigenvalue of the laplace operator, which corresponds to $m=n=0$, inequality (18) takes exactly the same form as the inequality that was necessary for (u_s, v_s) to be a spiral in the absence of diffusion, namely inequality (4). Therefore, to avoid repetition the stability analysis of the steady state (u_s, v_s) with $m=n=0$ is skipped and the non-trivial case is studied, i.e. $m, n\geq 1$.

Conditions (34) has consequences in terms of the stability of the original system. The first consequence is that if $\lambda_{1,2}$ have imaginary parts, then condition (34) guarantees that the real part of $\lambda_{1,2}$ is negative for all choices of α and β, allowing the eigenvalues to be positive if and only if they are both real repeated or real distinct (with at least one of them positive). Hence, restricting the system from undergoing *Hopf* bifurcation. Similarly, if $\lambda_{1,2}$ have imaginary parts, then condition (34) must be violated (condition (23) must be satisfied) in order for the real part of $\lambda_{1,2}$ to become positive whilst the eigenvalues are still complex conjugate pair. It means that for the original system to undergo *Hopf* bifurcation, the necessary condition on the domain size is (23). If both eigenvalues are negative distinct real values, then the system is spatially as well as temporally stable, the dynamics will achieve no patterns, hence the system returns to the uniform constant steady state (u_s, v_s) as time grows, [see Section 5 Fig. 11] with no effect from diffusion. If the eigenvalues are both real with different signs, then the type of instability caused by diffusion is spatially periodic or oscillatory in space, because this case corresponds to the steady state becoming

a saddle point. If both eigenvalues are positive real distinct values, then the dynamics are expected to exhibit a spatially periodic pattern, in the form of stripes or spots. Condition (34) is formally proven in Theorem 2, where it is shown that for a domain size satisfying (34) the dynamics of the system with diffusion is expected to undergo spatial patterning only.

Theorem 2 (Turing type diffusion-driven instability)**.** *Let u and v satisfy the non-dimensional reaction-diffusion system with* activator-depleted *reaction kinetics (1) on a square domain* $\Omega \subset \mathbb{R}^2$ *with area* L^2 *and positive parameters* $\gamma > 0$, $d > 0$, $\alpha > 0$ *and* $\beta > 0$. *Given that the area of the square domain* $\Omega \subset \mathbb{R}^2$ *satisfies the inequality*

$$L^2 < \pi^2 \frac{(d+1)(m^2+n^2)}{\gamma}, \tag{34}$$

where $m, n \in \mathbb{N}$ *then for all* $\alpha, \beta \in \mathbb{R}_+$ *in the neighbourhood of the unique steady state* $(u_s, v_s) = \left(\alpha+\beta, \frac{\beta}{(\alpha+\beta)^2}\right)$ *the diffusion driven instability is restricted to Turing type only, forbidding the existence of Hopf and transcritical bifurcation.*

Proof. The strategy of this proof is through detailed analysis of the real part of the eigenvalues of the linearised system, when $\lambda_{1,2} \in \mathbb{C}\backslash\mathbb{R}$. This can be done through studying the surface $\mathcal{T}(\alpha, \beta)$, and finding that it has a unique extremum point at (0, 0). The method of second derivative test and Hessian matrix is used to determine the type of this extremum. Upon finding its type, then the monotonicity of $\mathcal{T}(\alpha, \beta)$ is analysed in the neighbourhood of the extremum point in both directions α and β. The monotonicity analysis and the type of the extremum leads to proving the claim of the theorem.

The eigenvalues $\lambda_{1,2}$ in the presence of diffusion, in terms of trace $\mathcal{T}(\alpha, \beta)$ and determinant $\mathcal{D}(\alpha, \beta)$ are given by $\lambda_{1,2} = \frac{1}{2}\mathcal{T}(\alpha, \beta) \pm \frac{1}{2}\sqrt{\mathcal{T}^2(\alpha, \beta) - 4\mathcal{D}(\alpha, \beta)}$, where

$$\mathcal{T}(\alpha, \beta) = \gamma \frac{\beta - \alpha - (\beta+\alpha)^3}{\beta+\alpha} - (d+1)\frac{(n^2+m^2)\pi^2}{L^2},$$

$$\mathcal{D}(\alpha, \beta) = \left(\gamma\frac{\beta-\alpha}{\beta+\alpha} - \frac{(n^2+m^2)\pi^2}{L^2}\right) \times \left(-\gamma(\beta+\alpha)^2 - d\frac{(n^2+m^2)\pi^2}{L^2}\right) + 2\gamma^2\beta(\beta+\alpha).$$

It can be immediately observed that in the neighbourhood of (u_s, v_s) for the system to exhibit Hopf or transcritical bifurcation the discriminant of the characteristic polynomial must satisfy the inequality $\mathcal{T}^2(\alpha, \beta) - 4\mathcal{D}(\alpha, \beta) < 0$. Therefore, the stability and type of the steady state (u_s, v_s) in this case is determined by the sign of the real part of $\lambda_{1,2}$. The aim is to investigate $\mathcal{T}(\alpha, \beta)$ and derive from it condition (34) on L^2 as a requirement for $\mathcal{T}(\alpha, \beta)$ to be negative for all strictly positive choices of γ, α, β and $d > 0$. First derivative test is used on $\mathcal{T}(\alpha, \beta)$ to find all stationary points of $\mathcal{T}(\alpha, \beta)$ on the domain $[0, \infty) \times [0, \infty)$. All stationary points of $\mathcal{T}(\alpha, \beta)$ must satisfy $\frac{\partial \mathcal{T}}{\partial \alpha} = -\gamma\frac{2(\alpha+\beta)^3+2\beta}{(\alpha+\beta)^2} = 0$, which is true if and only if

$$(\alpha+\beta)^3 + \beta = 0. \tag{35}$$

Similarly all stationary points of $\mathcal{T}(\alpha, \beta)$ must also satisfy $\frac{\partial \mathcal{T}}{\partial \beta} = -\gamma\frac{2(\alpha+\beta)^3-2\alpha}{(\alpha+\beta)^2} = 0$, which implies

$$(\alpha+\beta)^3 - \alpha = 0. \tag{36}$$

The system of nonlinear algebraic equations obtained from (35) and (36) has a unique solution namely $\alpha = 0$ and $\beta = 0$ [see Remark 3.2.1]. Therefore, $\mathcal{T}(\alpha, \beta)$ has a unique stationary point at the origin. The type of this stationary point is determined by the second derivative test for which the Hessian matrix $H(\mathcal{T}(\alpha, \beta))$ must be computed and evaluated at the point (0, 0).

$$H(\mathcal{T}(\alpha,\beta))|_{(0,0)} = \begin{bmatrix} \frac{\partial^2\mathcal{T}}{\partial\alpha^2} & \frac{\partial^2\mathcal{T}}{\partial\beta\partial\alpha} \\ \frac{\partial^2\mathcal{T}}{\partial\alpha\partial\beta} & \frac{\partial^2\mathcal{T}}{\partial\beta^2} \end{bmatrix}_{(0,0)} = \begin{bmatrix} -\gamma\frac{4\beta-2(\alpha+\beta)^3}{(\alpha+\beta)^3} & -\gamma\frac{2(\alpha+\beta)^3+2(\alpha-\beta)}{(\alpha+\beta)^3} \\ -\gamma\frac{2(\alpha+\beta)^3+2(\alpha-\beta)}{(\alpha+\beta)^3} & -\gamma\frac{2(\alpha+\beta)^3+4\alpha}{(\alpha+\beta)^3} \end{bmatrix}_{(0,0)}.$$

It is clear that the entries of H upon direct evaluation at the point (0, 0) are undefined. This is treated by using L'Hopital's rule. L'Hopital's rule sometimes does not work for functions of two variables defined on cartesian coordinates, therefore a transformation of the entries to polar coordinates might be applied. We will exploit this technique to express the Hessian matrix in polar coordinates and differentiate accordingly. The entries of H are transformed to polar coordinates using $\alpha = r\cos(\theta)$ and $\beta = r\sin(\theta)$, so the rule can be applied by taking the $\lim_{r\to 0} H$. Using (r, θ) coordinates the entries of H take the following form

$$H(\mathcal{T}(r,\theta))|_{r=0} = -\gamma\begin{bmatrix} \frac{4r\sin\theta - 2r^3(\cos\theta+\sin\theta)^3}{r^3(\cos\theta+\sin\theta)^3} & \frac{2r^3(\cos\theta+\sin\theta)^3+2r(\cos\theta-\sin\theta)}{r^3(\cos\theta+\sin\theta)^3} \\ \frac{2r^3(\cos\theta+\sin\theta)^3+2r(\cos\theta-\sin\theta)}{r^3(\cos\theta+\sin\theta)^3} & \frac{4r\cos\theta+2r^3(\cos\theta+\sin\theta)^3}{r^3(\cos\theta+\sin\theta)^3} \end{bmatrix}_{r=0}. \tag{37}$$

L'Hopital's rule is applied to each entry of H separately and the $\lim_{r\to 0} H_{ij}(\mathcal{T}(r,\theta))$ is computed for $i, j = 1, 2$. Starting with the entry H_{11} and cancelling r, the expression takes the form

$$\lim_{r\to 0} H_{11} = \lim_{r\to 0} \frac{4\sin\theta - 2r^2(\cos\theta+\sin\theta)^3}{r^2(\cos\theta+\sin\theta)^3}.$$

Let $\mathcal{T}_1(r,\theta)$ and $\mathcal{T}_2(r,\theta)$ respectively denote the numerator and the denominator of the expression for H_{11}, then the application of L'Hopital's rule suggests that

$$\lim_{r\to 0} H_{11}(\mathcal{T}(r,\theta)) = \lim_{r\to 0}\frac{\mathcal{T}_1(r,\theta)}{\mathcal{T}_2(r,\theta)} = \frac{\lim_{r\to 0}\frac{d\mathcal{T}_1}{dr}(r,\theta)}{\lim_{r\to 0}\frac{d\mathcal{T}_2}{dr}(r,\theta)} = \lim_{r\to 0}\frac{-4r(\cos\theta+\sin\theta)^3}{2r(\cos\theta+\sin\theta)^3} = -2.$$

Applying the same procedure for H_{12}, H_{21} and H_{22}, all the entries of H are computed and given by

$$H(\mathcal{T}(\alpha,\beta))|_{(0,0)} = -\gamma\begin{bmatrix} -2 & 2 \\ 2 & 2 \end{bmatrix}. \tag{38}$$

Since the $\det(H) = -8\gamma^2 < 0$, therefore, the second derivative test suggests that (0, 0) is a saddle point of $\mathcal{T}(\alpha, \beta)$. Since it was previously shown that $\mathcal{T}(\alpha, \beta)$ attains a unique stationary point in the domain $[0, \infty) \times [0, \infty)$, i.e. by solving the Eqs. (35) and (36), therefore, if (0, 0) was a maximum and $\mathcal{T}(0, 0) < 0$, this would suggest that, whenever $\lambda_{1,2}$ has a non-zero imaginary part then $Re(\lambda_{1,2}) < 0$ regardless of the choice of d, γ and L^2, however due to fact that (0, 0) is a saddle point, it remains to show that $\mathcal{T}(\alpha, \beta)$ is negative at (0, 0) and its first derivatives in the neighbourhood of (0, 0) of $\mathcal{T}(\alpha, 0)$ and $\mathcal{T}(0, \beta)$ for positive values of α and β in both directions are negative and do not change sign. Let $\mathcal{T}_0(\alpha)$ and $\mathcal{T}_0(\beta)$ denote the curves for constants $\beta = 0$ and $\alpha = 0$ respectively

on the plane $\mathcal{T}(\alpha,\beta)$, then

$$\mathcal{T}_0(\alpha)=\lim_{\beta\to 0}\mathcal{T}(\alpha,\beta)=-\gamma(1+\alpha^2)-(d+1)\frac{(m^2+n^2)\pi^2}{L^2},$$

$$\mathcal{T}_0(\beta)=\lim_{\alpha\to 0}\mathcal{T}(\alpha,\beta)=\gamma(1-\beta^2)-(d+1)\frac{(m^2+n^2)\pi^2}{L^2}.$$

The expression for $\mathcal{T}_0(\alpha)$ clearly satisfy that it is negative at $\alpha=0$ and its first derivative in the direction of α is $\frac{d\mathcal{T}_0(\alpha)}{d\alpha}=-2\gamma\alpha<0$ for all $\gamma,\ \alpha\in[0,\infty)$. The expression for $\mathcal{T}_0(\beta)$ however is not trivially negative for all values, since the sign of the constant γ in the expression is positive, which if computed at $\beta=0$, leads to the desired condition

$$\mathcal{T}_0(\beta)\big|_{\beta=0}=\gamma-(d+1)\frac{(m^2+n^2)\pi^2}{L^2}<0$$
$$\iff \qquad L^2<\pi^2\frac{(d+1)(m^2+n^2)}{\gamma}.$$

It has been shown that the condition (34) is necessary for $\mathcal{T}(\alpha,\beta)$ to be negative at the unique stationary point namely (0, 0), it remains to show that the first derivative of $\frac{d\mathcal{T}_0}{d\beta}(\beta)<0$, $\frac{d\mathcal{T}_0}{d\beta}=-2\gamma\beta<0$ for all $\gamma\beta\in[0,\infty)$ which completes the proof. □

3.2.1. Remark

The parameters $(\alpha,\beta)=(0,0)$ are not the admissible choices for the original system, because this choice of parameters leads to the trivial steady state $(u_s,v_s)=(0,0)$, which is globally and unconditionally stable and has no physical relevance. However, the surface defined by $\mathcal{T}(\alpha,\beta)$, which determines the sign of the real part of $\lambda_{1,2}\in\mathbb{C}\backslash\mathbb{R}$ attains a unique extremum at (0, 0), which makes the analysis of the neighbourhood of this point important for studying the sign of $\mathcal{T}(\alpha,\beta)$. It is reasonable to argue that the point $(\alpha,\beta)=(0,0)$ is not permissible to use as the platform of the proof of Theorem 2, in that case, proving the results become a step closer by only showing that $\mathcal{T}(\alpha,\beta)$ is a strictly monotonically decreasing function (with no extrema in $(\alpha,\beta)\in\mathbb{R}^2_+$) and it can only attain bounded positive values in the neighbourhood of (0, 0) if and only if the condition (34) on the domain size L^2 is violated. Therefore, given that L^2 maintains to satisfy (34), the sign of the real part i.e. $\mathcal{T}(\alpha,\beta)$ of $\lambda_{1,2}\in\mathbb{C}\backslash\mathbb{R}$ is guaranteed to be negative, which is a step shorter to reach the claim of Theorem 2. Therefore, it is brought to the attention of the reader that the use of the point $(\alpha,\beta)=(0,0)$ as an extremum of $\mathcal{T}(\alpha,\beta)$ is more of complementary factor to the proof rather than an essential one.

3.3. Numerical solutions of the partitioning curves and parameter spaces

A similar numerical method to that used in the case of the absence of diffusion is applied to solve for the partitioning curves in the parameter plane. The partitioning curve separating real and complex regions, on the plane $(\alpha,\beta)\in\mathbb{R}_+$ must satisfy

$$\mathcal{T}^2(\alpha,\beta)-4\mathcal{D}(\alpha,\beta)=0, \tag{39}$$

since this is the curve on which the discriminant of the expression for eigenvalues change sign. Eq. (39) is solved by the same algorithm that was used to solve (6) on a square domain and for each fixed mesh point in the direction of α it is found that the solution of (39) is equivalent to finding the positive real roots of a six degree polynomial in β for fixed values of α_i in the form

$$\psi(\alpha_i,\beta)=C_0(\alpha_i)+C_1(\alpha_i)\beta+C_2(\alpha_i)\beta^2+C_3(\alpha_i)\beta^3+C_4(\alpha_i)\beta^4+C_5(\alpha_i)\beta^5+C_6(\alpha_i)\beta^6, \tag{40}$$

where for each α_i the coefficients are given by

$$\begin{aligned}C_0(\alpha_i)=\ & L^4\gamma^2{\alpha_i}^6+\big(4\,L^4\pi^2m^2+4\,L^4\pi^2n^2+2\,L^2\gamma\pi^2dm^2\\&+2\,L^2\gamma\pi^2dn^2+4\,L^6+2\,L^2\gamma\pi^2m^2\\&+2\,L^2\gamma\pi^2n^2+2\,L^4\gamma^2\big){\alpha_i}^4\\&+\big(-4\,L^2\pi^4dm^4-8\,L^2\pi^4dm^2n^2-4\,L^2\pi^4dn^4\\&-4\,L^2\pi^4m^4-8\,L^2\pi^4m^2n^2-4\,L^2\pi^4n^4-4\,L^4\pi^2dm^2\\&-4\,L^4\pi^2dn^2-4\,L^4\pi^2m^2-4\,L^4\pi^2n^2\big){\alpha_i}^3\\&+\big(\pi^4d^2m^4+2\,\pi^4d^2m^2n^2+\pi^4d^2n^4+2\,\pi^4dm^4\\&+4\,\pi^4dm^2n^2+2\,\pi^4dn^4+\pi^4m^4\\&+2\,\pi^4m^2n^2+\pi^4n^4+2\,L^2\gamma\pi^2dm^2+2\,L^2\gamma\pi^2dn^2\\&+2\,L^2\gamma\pi^2m^2+2\,L^2\gamma\pi^2n^2+L^4\gamma^2\big){\alpha_i}^2,\end{aligned}$$

$$\begin{aligned}C_1(\alpha_i)=\ & 6\,L^4\gamma^2{\alpha_i}^5-8\,L^4{\alpha_i}^4+\big(8\,L^4\pi^2m^2\\&+8\,L^4\pi^2n^2+8\,L^2\gamma\pi^2dm^2+8\,L^2\gamma\pi^2dn^2\\&+8\,L^2\gamma\pi^2m^2+8\,L^2\gamma\pi^2n^2+4\,L^4\gamma^2\big){\alpha_i}^3\\&+\big(-12\,L^2\pi^4dm^4-24\,L^2\pi^4dm^2n^2\\&-12\,L^2\pi^4dn^4-12\,L^2\pi^4m^4-24\,L^2\pi^4m^2n^2\\&-12\,L^2\pi^4n^4-4\,L^4\pi^2dm^2\\&-4\,L^4\pi^2dn^2-4\,L^4\pi^2m^2-4\,L^4\pi^2n^2\big){\alpha_i}^2\\&+\big(2\,\pi^4d^2m^4+4\,\pi^4d^2m^2n^2\\&+2\,\pi^4d^2n^4+4\,\pi^4dm^4+8\,\pi^4dm^2n^2+4\,\pi^4dn^4\\&+2\,\pi^4m^4+4\,\pi^4m^2n^2\\&+2\,\pi^4n^4-2\,L^4\gamma^2\big)\alpha_i,\end{aligned}$$

$$\begin{aligned}C_2(\alpha_i)=\ & 15\,L^4\gamma^2{\alpha_i}^4-32\,L^4{\alpha_i}^3+\big(12\,L^2\gamma\pi^2dm^2\\&+12\,L^2\gamma\pi^2dn^2-8\,L^6+12\,L^2\gamma\pi^2m^2+12\,L^2\gamma\pi^2n^2\big){\alpha_i}^2\\&+\big(-12\,L^2\pi^4dm^4-24\,L^2\pi^4dm^2n^2-12\,L^2\pi^4dn^4\\&-12\,L^2\pi^4m^4-24\,L^2\pi^4m^2n^2-12\,L^2\pi^4n^4\\&+4\,L^4\pi^2dm^2+4\,L^4\pi^2dn^2\\&+4\,L^4\pi^2m^2+4\,L^4\pi^2n^2\big)\alpha_i+\pi^4d^2m^4+2\,\pi^4d^2m^2n^2\\&+\pi^4d^2n^4+2\,\pi^4dm^4+4\,\pi^4dm^2n^2+2\,\pi^4dn^4+\pi^4m^4\\&+2\,\pi^4n^2m^2+\pi^4n^4-2\,L^2\gamma\pi^2dm^2-2\,L^2\gamma\pi^2dn^2\\&-2\,L^2\gamma\pi^2m^2-2\,L^2\gamma^2\pi^2n^2+L^4\gamma^2,\end{aligned}$$

$$\begin{aligned}C_3(\alpha_i)=\ & 20\,L^4\gamma^2{\alpha_i}^3-48\,L^4{\alpha_i}^2+\big(-8\,L^4\pi^2m^2-8\,L^4\pi^2n^2\\&+8\,L^2\gamma\pi^2dm^2+8\,L^2\gamma\pi^2dn^2+8\,L^2\gamma\pi^2m^2\\&+8\,L^2\gamma\pi^2n^2-4\,L^4\gamma\big)\alpha_i-4\,L^2\pi^4dm^4\\&-8\,L^2\pi^4dm^2n^2-4\,L^2\pi^4dn^4-4\,L^2\pi^4m^4\\&-8\,L^2\pi^4m^2n^2-4\,L^2\pi^4n^4\\&+4\,L^4\pi^2dm^2+4\,L^4\pi^2dn^2+4\,L^4\pi^2m^2+4\,L^4\pi^2n^2,\end{aligned}$$

$$\begin{aligned}C_4(\alpha_i)=\ & 15\,L^4\gamma^2{\alpha_i}^2-32\,L^4\alpha_i-4\,L^4\pi^2m^2-4\,L^4\pi^2n^2\\&+2\,L^2\gamma\pi^2dm^2+2\,L^2\gamma\pi^2dn^2+4\,L^6+2\,L^2\gamma\pi^2m^2\\&+2\,L^2\gamma\pi^2n^2-2\,L^4\gamma^2,\end{aligned}$$

$$C_5(\alpha_i)=6\,L^4\gamma^2\alpha_i-8\,L^4, \quad \text{and} \quad C_6(\alpha_i)=\gamma^2L^4.$$

The implicit curve satisfying (40) indicates the choices of $(\alpha,\ \beta)$ for which the eigenvalues are repeated real roots. The polynomial $\psi_i(\beta)$ of degree six, given by (40) is solved for 5000 fixed α_i on a

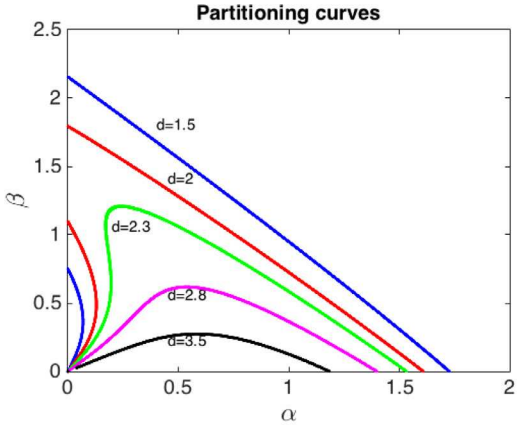

(a) Boundary curves for complex $\lambda_{1,2}$ with corresponding values of d and the condition $L^2 = 25 < \pi^2 \frac{(d+1)(m^2+n^2)}{\gamma}$.

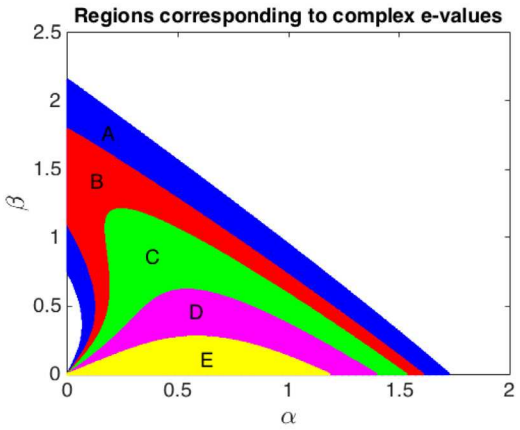

(b) Regions corresponding to complex eigenvalues associated to values of d indicated in Figure (a) and condition (34).

Fig. 6. Parameter regions corresponding to complex eigenvalues and their boundary curves for various values of d and domain size L restricted to the condition (34) of Theorem 2.

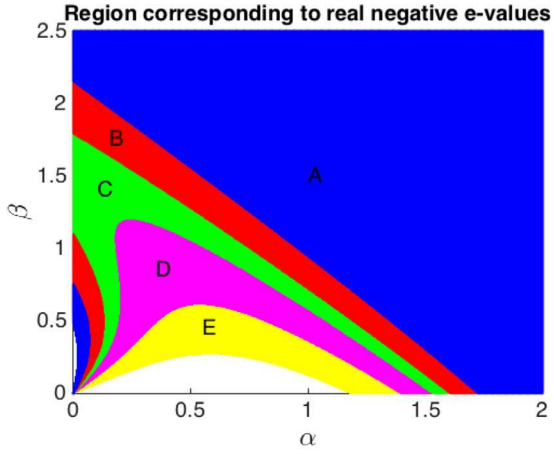

(a) Regions where $\lambda_{1,2}$ are both real and negative.

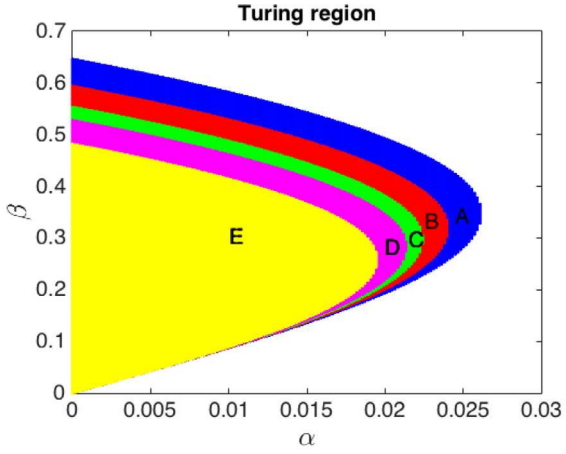

(b) Regions where both eigenvalues are real and at least one of λ_1 or λ_2 are positive.

Fig. 7. The region where $\lambda_{1,2}$ are both real for various values of d and domain size L^2 restricted to the condition (34) in Theorem 2.

domain with $\alpha_{\max} = \beta_{\max} = 3$. For each α_i the positive real roots of $\psi_i(\beta)$ are extracted and plotted on the $(\alpha, \beta) \in \mathbb{R}_+$ plane. The algorithm is run for five different values of the non-dimensional parameter d, associated to both cases, where the area L^2 of Ω satisfies condition (34) of Theorem 2 as well as condition (23) of Theorem 1.

The equation for the second curve that partitions the region corresponding to complex eigenvalues of the parameter plane is the curve on which the real parts of the complex roots are zero, hence satisfying the equation

$$\mathcal{T}(\alpha, \beta) = \gamma \frac{\beta - \alpha - (\alpha + \beta)^3}{\beta + \alpha} - \frac{(d+1)(m^2+n^2)\pi^2}{L^2} = 0. \quad (41)$$

The solution of (41) by algebraic manipulation can be found to be equivalent to finding the positive real roots of the cubic polynomial $\phi(\alpha_i, \beta) = 0$ for fixed α_i, where ϕ is given by

$$\phi(\alpha_i, \beta) = C_0(\alpha_i) + C_1(\alpha_i)\beta + C_2(\alpha_i)\beta^2 + C_3(\alpha_i)\beta^3, \quad (42)$$

with $C_0(\alpha_i) = -\left(L^2\gamma + (d+1)(n^2+m^2)\pi^2\right) - L^2\gamma\alpha_i^3, C_1(\alpha_i) = L^2\gamma - (d+1)(n^2+m^2)\pi^2 - 3L^2\gamma\alpha_i^2, C_2(\alpha_i) = -3L^2\gamma\alpha_i,$ and $C_3(\alpha_i) = -L^2\gamma$.

Variations of the parameter d are investigated, whilst the area L^2 remains to satisfy condition (34) and as expected it is found that in the region of the parameter plane corresponding to complex eigenvalues, there is no sub-region that corresponds to $\lambda_{1,2}$ to have positive real parts. For each value of d the region corresponding to complex eigenvalues is tested by looking for a critical curve on which $\lambda_{1,2}$ is purely imaginary, i.e. satisfying (42). If such a curve exists, it would correspond to the system undergoing periodic oscillations around (u_s, v_s), thus the system exhibiting transcritical bifurcation, which also implies the existence of a region in the parameter space that corresponds to real parts of $\lambda_{1,2}$ to be positive. Upon investigating this region, it is found that such a curve under condition (34) does not exists, and all roots corresponding to the cubic polynomial given by (42) are either complex eigenvalues or they are negative real values, therefore cannot be the choice of admissible parameters of the system. Another observation is that

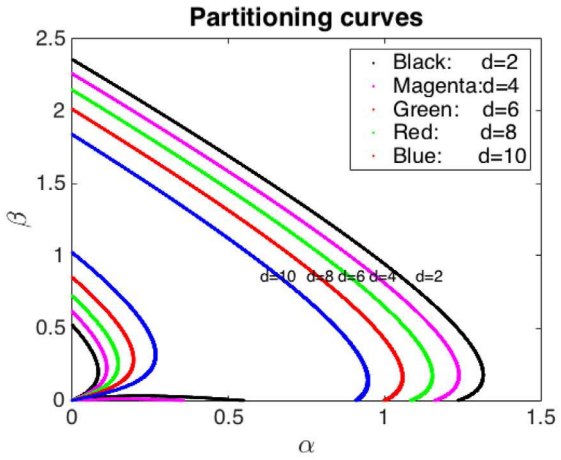

(a) Boundary curves for complex $\lambda_{1,2}$ with corresponding values of d and the condition $L^2 = 225 > \pi^2 \frac{(d+1)(m^2+n^2)}{\gamma}$.

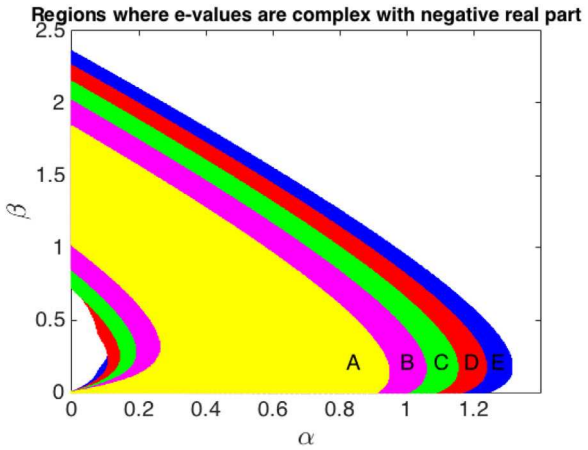

(b) Regions corresponding to complex eigenvalues associated to values of d indicated in Figure (a) and condition (23).

Fig. 8. Parameter regions corresponding to complex eigenvalues and their boundary curves for various values of d and domain size L restricted to the condition (23) of Theorem 1.

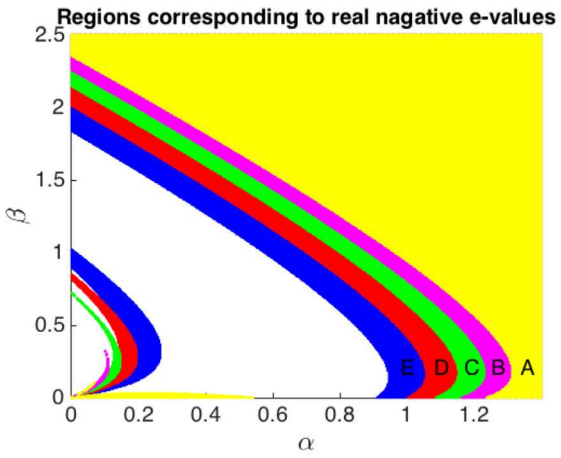

(a) Regions where $\lambda_{1,2}$ is real distinct and negative.

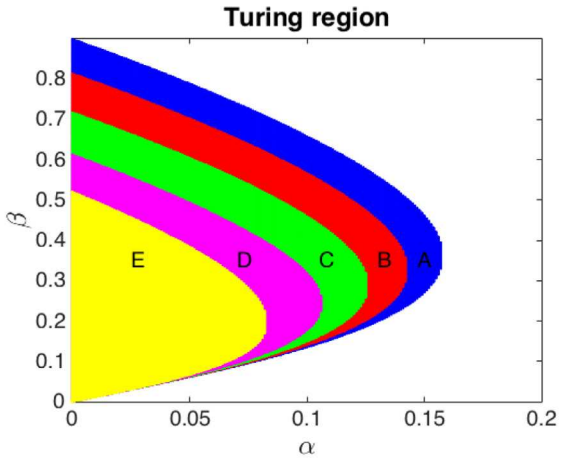

(b) Region where $\lambda_{1,2}$ are real distinct and at least one of them positive.

Fig. 9. Different colours denoted by capital letters indicate the regions of stability of the model system (1) for their corresponding values of d. (For interpretation of the references to colour in this figure legend, the reader is referred to the web version of this article.).

as d increases the area of the region corresponding to complex eigenvalues in the (α, β) plane gradually decreases. The domain size of length $L = 5$ satisfying the condition of Theorem 2 is tested for stability analysis of (u_s, v_s) when $\lambda_{1,2}$ are complex eigenvalues. The results are shown for different values of d by a distinct colour in Fig. 4 (a). Finding the solutions of these curves does not however indicate, which side of them correspond to complex $\lambda_{1,2}$ and which side to real $\lambda_{1,2}$. This is decided by some numerical trial and error by evaluating $\lambda_{1,2}$ using few values from both sides of each curve. Trial and error indicates that the regions under these curves correspond to $\lambda_{1,2}$ to be a complex conjugate pair and hence any combination of (α, β) from this region ensures that the eigenvalues $\lambda_{1,2}$ contain a non-zero imaginary part. When the area L^2 of Ω satisfies condition (34), the absence of a region satisfying (42) verifies the statement of Theorem 2, therefore the region corresponding to complex eigenvalues for the choice of L^2 satisfying (34) has no sub-partitions, because everywhere in this region the real part of the eigenvalues is negative, hence no choice of parameters could result in the system to exhibit Hopf or transcritical bifurcation. The eigenvalues only become positive when they are both real values, therefore condition (34) restricts the diffusion-driven instability to Turing type only. Fig. 6 (a) shows how the partitioning curve changes location, as the value of d is varied. The region under those curves corresponds to the complex eigenvalues. Similarly Fig. 6 (b) indicates the regions corresponding to complex eigenvalues for the corresponding values of d. Each stripe in Fig. 6 (b) is denoted by a letter that represents the set of all points corresponding to a distinct colour stripe. Similarly, the regions where the eigenvalues $\lambda_{1,2}$ are negative real roots are presented by Fig. 7 (a), corresponding to the same values of the parameter d. Fig. 7 (b) shows regions where at least one or both eigenvalues are positive real roots. The summary of Figs. 6 and 7 is presented in Table 2.

The algorithm is also run for the case when L^2 is chosen such that it satisfies (23) and we find that the region corresponding to

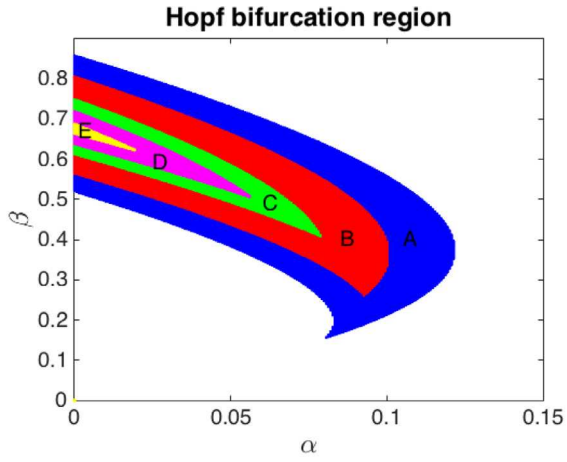

(a) Region for complex $\lambda_{1,2}$ and positive real part with corresponding values of d and the condition $L^2 = 225 > \pi^2 \frac{(d+1)(m^2+n^2)}{\gamma}$.

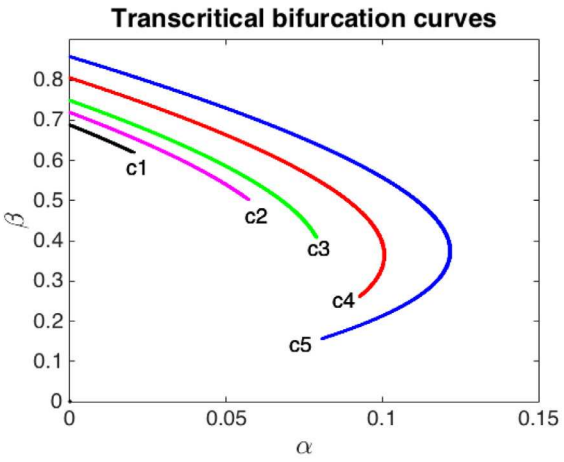

(b) Regions corresponding to complex eigenvalues associated to values of d indicated in Figure (a) and condition (23).

Fig. 10. Parameter regions corresponding to complex eigenvalues and their boundary curves for various values of d and domain size L restricted to the condition (23) of Theorem 1.

Table 2
Table showing regions corresponding to domain size $L^2 < \frac{\pi^2(d+1)(m^2+n^2)}{\gamma}$, which satisfies (34) of Theorem 2.

Plot index	Fig. 7 (a)	Fig. 7 (b)	Fig. 6 (b)	Fig. 6 (b)	Fig. 6 (b)
Eigenvalues Value of d\Type of (SS)	$0 > \lambda_{1,2} \in \mathbb{R}$ Stable node	$0 < \lambda_{1,2} \in \mathbb{R}$ Turing type instability	$\lambda \in \mathbb{C}, Re(\lambda_{1,2}) < 0$ Stable spiral	$\lambda \in \mathbb{C}, Re(\lambda_{1,2}) > 0$ Hopf bifurcation	$\lambda \in \mathbb{C}, Re(\lambda) = 0$ Transcritical bifurcation
1.5	A	E	$A \cup B \cup C \cup D \cup E$	$\emptyset$	$\emptyset$
2	$A \cup B$	$E \cup D$	$B \cup C \cup D \cup E$	$\emptyset$	$\emptyset$
2.3	$A \cup B \cup C$	$E \cup D \cup C$	$C \cup D \cup E$	$\emptyset$	$\emptyset$
2.8	$A \cup B \cup C \cup D$	$E \cup D \cup C \cup B$	$D \cup E$	$\emptyset$	$\emptyset$
3.5	$A \cup B \cup C \cup D \cup E$	$E \cup D \cup C \cup B \cup A$	E	$\emptyset$	$\emptyset$

Table 3
Table showing regions corresponding to the domain size $L^2 = 225 \geq \frac{\pi^2(d+1)(m^2+n^2)}{\gamma}$, which satisfies (23) of Theorem 1.

Plot index	Fig. 9(a)	Fig. 9(b)	Fig. 8(b)	Fig. 10(a)	Fig. 10(b)
Eigenvalues Value of d\Type of (SS)	$0 > \lambda_{1,2} \in \mathbb{R}$ Stable node	$0 < \lambda_{1,2} \in \mathbb{R}$ Turing type instability	$\lambda \in \mathbb{C}, Re(\lambda_{1,2}) < 0$ Stable spiral	$\lambda \in \mathbb{C}, Re(\lambda_{1,2}) > 0$ Hopf bifurcation	$\lambda \in \mathbb{C}, Re(\lambda) = 0$ Transcritical bifurcation
2	A	E	$A \cup B \cup C \cup D \cup E$	$A \cup B \cup C \cup D \cup E$	c_5
4	$A \cup B$	$E \cup D$	$B \cup C \cup D \cup E$	$B \cup C \cup D \cup E$	c_4
6	$A \cup B \cup C$	$E \cup D \cup C$	$C \cup D \cup E$	$C \cup D \cup E$	c_3
8	$A \cup B \cup C \cup D$	$E \cup D \cup C \cup B$	$D \cup E$	$D \cup E$	c_2
10	$A \cup B \cup C \cup D \cup E$	$E \cup D \cup C \cup B \cup A$	E	E	c_1

complex eigenvalues is further partitioned by the curve satisfying (41). This is the curve on which the eigenvalues are purely imaginary. This curve also indicates that within the region corresponding to complex eigenvalues there is a sub-region in which the eigenvalues are complex with positive real part, which corresponds to the system exhibiting Hopf bifurcation. For choices of parameter values on the curve the system is expected to undergo transcritical bifurcation. The area of the domain Ω is taken as $L^2 = 225$ in order to satisfy the condition given by Theorem 1 with respect to d and γ, so that there is enough space for varying d and yet maintaining condition (23). It can be easily observed from the parameter space classification that there is a relatively small region in each case corresponding to diffusion-driven instability. This indicates the importance of making sure to choose parameter choices wisely, in order to expect the dynamics of the system to evolve to certain types of patterns or maybe no patterns at all. Table 3 presents the summary for how the regions of the parameter space change with varying the parameter d. It would be reasonable to use the same variation of the parameter d in both cases of the domain sizes, however, in the first case where the domain size satisfies (34) the span of varying parameter d is relatively small, yet causing significant observable change in the parameter space. However, when the domain size is chosen according to condition (23), small variations in the diffusion coefficient makes insignificant changes to the parameter spaces, therefore, in order to pictorially observe the consequential change in the parameter plane (α, β) the span of variations for d have to be significantly large as seen in Table 2.

In the case when L^2 satisfies Theorem 2, it can be observed that the type of diffusion-driven instability that can occur is restricted to Turing type only, which is increased as the non-dimensional diffusion coefficient d was increased. Turing diffusion-driven instability also occurs for the case when L^2 satisfies condition (23) and it also increases with increased value of d as shown in Fig. 9(b). The interpretation is that regions in the parameter space exist, which

Table 4
Showing the choice of parameters (α, β) for each simulation and the choice of (d, γ) subject to the relevant condition referred to in third row. Each simulation was run with time-step of 1×10^{-3}.

Plot index	Fig. 11	Fig. 12	Fig. 13	Fig. 14
Parameters\Instability	No instability No pattern	Turing type instability Spatial pattern	Turing type instability Spatial pattern	Hopf bifurcation Spatial and temporal pattern
(α, β)	(2, 2)	(0.025, 0.4)	(0.1, 0.6)	(0.05, 0.8)
(d, γ)	(10, 210)	(10, 210)	(10, 300)	(10, 350)
Condition on Ω	(34)	(34)	(23)	(23)
Simulation time	2	4	4	6
CPU time (sec)	77.14	149.60	149.55	215.02

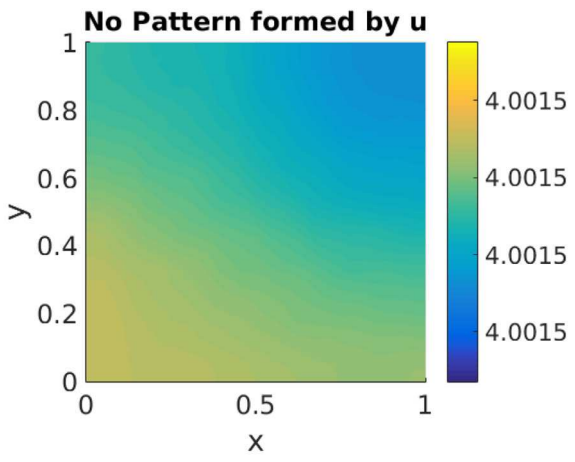

(a) The evolved discrete solution U at the final time step $T = 2$.

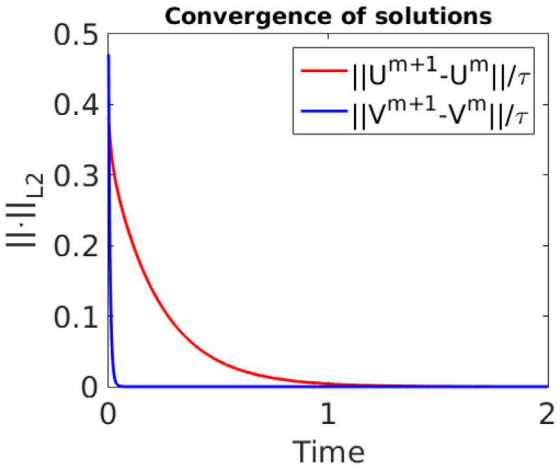

(b) Convergence in the L_2 norm of the discrete time derivative of the solutions U and V.

Fig. 11. Finite element numerical simulations corresponding to the u of the model system (1) with parameter values α and β selected from outside the Turing space (see Table 4 for values) and domain size satisfying (34). No patterns are obtained in agreement with the theoretical predictions.

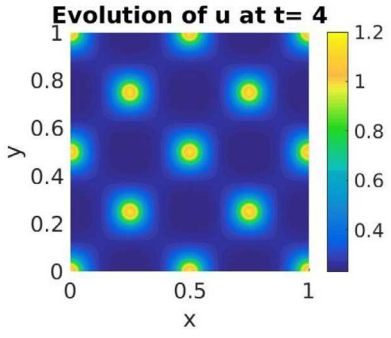

(a) The evolved discrete solution U at the final time step $T = 4$.

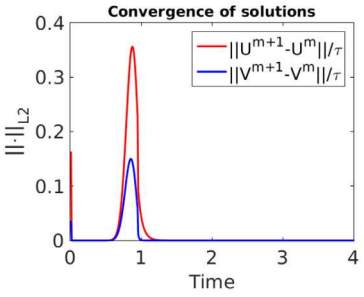

(b) Convergence in the L_2 norm of the discrete time derivative of the solutions U and V.

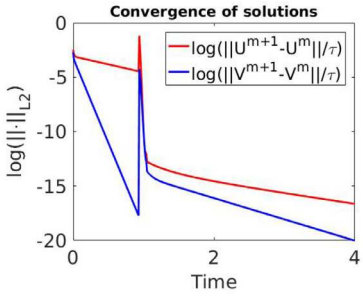

(c) Logarithmic convergence in the L_2 norm of the discrete time derivative of the solutions U and V.

Fig. 12. Finite element numerical simulations corresponding to the u of the model system (1) with parameter values α and β selected from the Turing space (see Table 4 for values) and domain size satisfying (34). We observe the formation of spot patterns, again in agreement with the theoretical predictions.

result in the system to be stable in the absence of diffusion, but when diffusion is added to the system, the choice of the parameters from these particular regions result in the system exhibiting instability. This type of instability is restricted to space and hence leads to spatial patterning only, because the eigenvalues are both real. However, if L^2 satisfies (23), then in addition to the existence of regions of the parameter space corresponding to Hopf and transcritical bifurcations, it can also be observed that with increased values of parameter d, unlike Turing instability, the regions for Hopf and transcritical bifurcations reduce as shown in Fig. 10(a) and (b). The mathematical intuition for this inverse relation is the direct proportionality of d on the lower bound for the domain size i.e. the right-hand side of (23). Therefore, as d grows, one gets closer to the violation of the necessary condition (23) for Hopf and transcritical bifurcations as proposed by Theorem 1. However, the region for Hopf and transcritical bifurcations remains to exist as long as L^2 satisfies (23), which ultimately means that for the system to exhibit temporal periodicity (patterning in time) the domain size has to be sufficiently large satisfying (23).

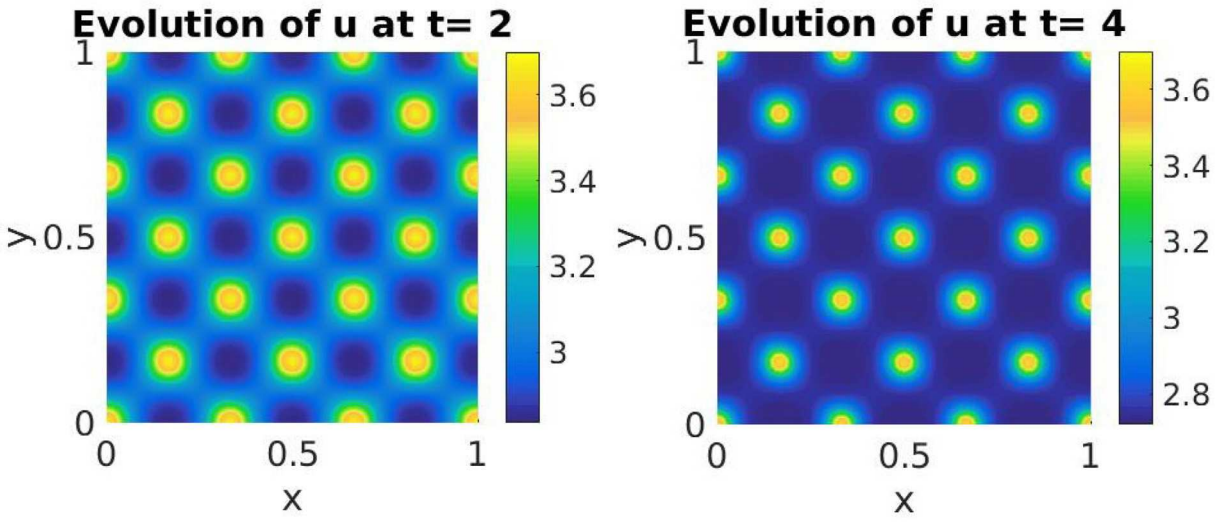

(a) The evolving discrete solution U captured at time step $t = 2$.

(b) The evolved discrete solution U captured at final time step $t = 4$.

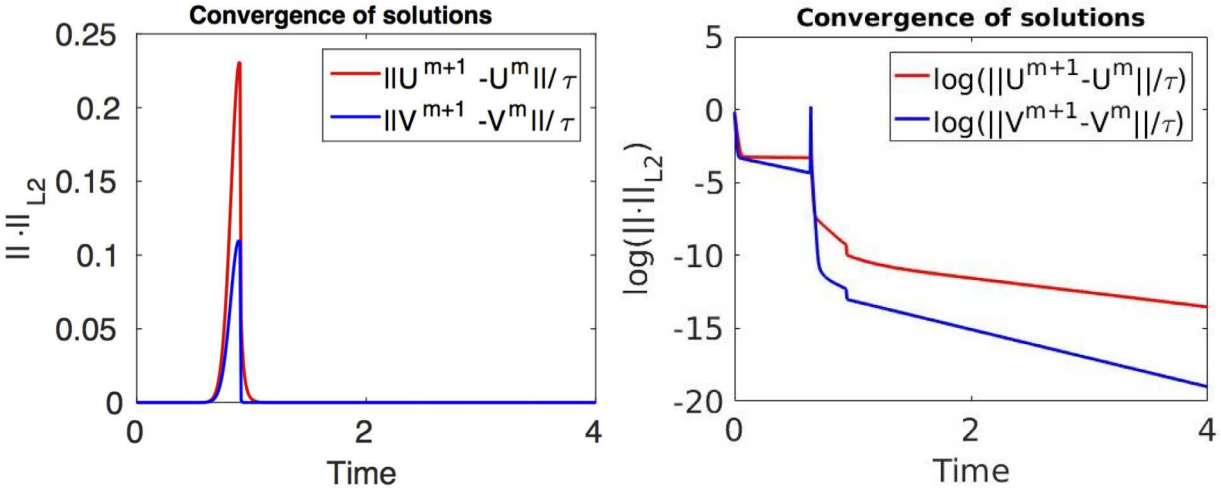

(c) Convergence in the L_2 norm of the discrete time derivative of the solutions U and V.

(d) Logarithmic convergence in the L_2 norm of the discrete time derivative of the solutions U and V.

Fig. 13. Finite element numerical simulations corresponding to the u of the model system (1) with parameter values α and β selected from the Turing space (see Table 4 for values) and domain size satisfying (23). We observe the formation of spot patterns which are more clustered than those obtained in Fig. 12.

3.3.1. Remark

The eigenfunction modes used for the current simulations corresponds to the first non-trivial (non-zero) eigenvalues, namely the case where $m = n = 1$. The results can be readily obtained for any positive integer values of m and n. Despite the fact that using larger integer values for m and n will shift or scale the classification for the parameter space, the conditions given by Theorems 2 and 1 will remain intact irrespective of the values of m and n, so long as they are positive integers.

4. Finite element numerical solutions

To validate the proposed classification of parameter space, the reaction-diffusion system (1) is numerically solved using the finite element method [1,5,9,40] on a unit square domain with a uniform triangular mesh. Numerical simulations are performed for various choices of parameter values α and β, chosen from the appropriate parameter spaces to demonstrate and validate our theoretical findings. In all our simulations, we vary the parameters d and γ and keep fixed the domain length size L and this allows us to keep constant the well refined number of degrees of freedom for the mesh. The initial conditions for each simulation are taken as small random perturbations around the neighbourhood of the steady state of the form [19,41]

$$\begin{cases} u_0(x,y) = \alpha + \beta + 0.0016\cos(2\pi(x+y)) + 0.01\sum_{i=1}^{8}\cos(i\pi x), \\ v_0(x,y) = \frac{\beta}{(\alpha+\beta)^2} + 0.0016\cos(2\pi(x+y)) + 0.01\sum_{i=1}^{8}\cos(i\pi x). \end{cases} \tag{43}$$

The final time T is chosen to ensure that beyond T the convergence of solutions in successive time-step differences decay to a threshold of 10^{-5} for all the simulations. Therefore, in the case where the area L^2 of the domain size satisfies condition (34) proven in Theorem 2, when temporal instability is forbidden by the condition on the domain size, the final time of numerical simulations is relatively shorter compared to that used for other cases. For numerical

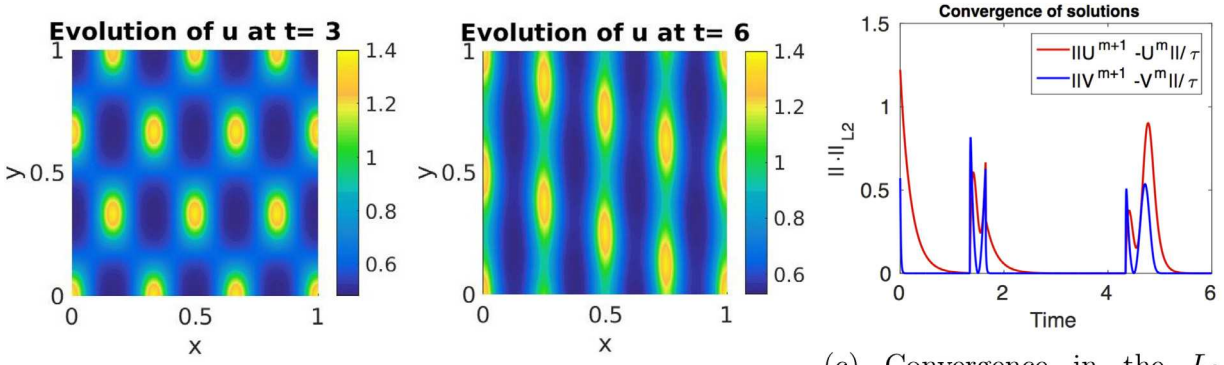

(a) The evolving discrete solution U captured at time step $t = 3$.

(b) The evolved discrete solution U captured at final time step $t = 6$.

(c) Convergence in the L_2 norm of the discrete time derivative of the solutions U and V.

Fig. 14. Finite element numerical simulations corresponding to the u of the model system (1) with parameter values α and β selected from the Hopf/Transcritical bifurcation region (see Table 4 for values) and domain size satisfying (23). We observe the formation of spatial-temporal periodic patterning in agreement with theoretical predictions.

simulations on the domain size L^2 satisfying condition (23) proven in Theorem 1, the final time is experimented for longer periods to capture possible existence of temporal periodicity in the dynamics. Simulations with domain size satisfying (23) are captured at different times, which varies with cases, for which details are included in Table 4. In all our numerical results, we only exhibit numerical solutions corresponding to the $u(x, y, t)$ component, those of $v(x, y, t)$ are known to be 180° out of phase to those of u [20].

Fig. 11 presents the case where the parameters $\alpha = 2$ and $\beta = 2$ are chosen from stable node region of Table 2, with final time $T = 2$. It can be observed that the evolved profile of the concentration u uniformly converges to the steady state value forming neither spatial nor temporal patterns (Fig. 11(a)). As predicted in Theorem 2, no choice of parameters α and β can influence the dynamics to exhibit temporal periodicity, therefore any choice of the parameters outside Turing space, given that the domain size satisfies (34) will uniformly converge to the stable steady state $(u_s, v_s) = (\alpha + \beta, \frac{\beta}{(\alpha+\beta)^2}) \approx (4, 0.125)$ as seen in Fig. 11(a). Fig. 11(b) shows the uniform convergence of the discrete L_2-norm difference between solutions at successive time-steps to the constant steady state (u_s, v_s), where there is no sign of instability occurring, when parameters are outside the Turing space.

Fig. 12(a) presents the evolved profile of the solution captured at the final time step, for the choice of parameters from Turing space presented in Table 4. The convergence in the discrete L_2-norm of difference in the solutions for the successive time steps from start to the end of the simulations are also plotted against time and presented in Fig. 12(b).

Fig. 13 shows the simulation for the choice of parameters from the Turing space presented in Table 3 for the domain size satisfying (23). In this case as predicted in Theorem 1, regions of parameter space exist for which the dynamic can exhibit Hopf type bifurcation, therefore, the possibility of temporal periodicity in the dynamics. Fig. 14 presents such periodicity in time for spatial patterns. The relative discrete L_2-norm of the difference in the solutions for successive time-steps is therefore showing time periodicity as illustrated in Fig. 14(d), which indicates the transition of the solution from the initially achieved spatial pattern to a different spatial pattern.

5. Conclusion

In this work the full parameter space for a reaction-diffusion system with *activator-depleted* reaction kinetics was classified through the use of linear stability theory and in each region of the parameter space the dynamics of the reaction-diffusion system was verified to exhibit the predicted type of behaviour. In the absence of diffusion, theoretical results on the dynamics of the system were supported by use of the phase-plane analysis, where in each case the numerical solution of the system was observed to be in agreement with the theoretically predicted behaviour. In the presence of diffusion, for a two-component reaction-diffusion system, two conditions relating the domain size to the diffusion and reaction rates were derived. The proofs of these conditions were presented in Theorems 1 and 2, respectively. For full classification of the parameter space, a numerical method was used to compute the solutions of the implicit curves in the parameter space forming the partitions of classification. In particular, using condition (34) the numerical method for solving the partitioning curves showed the non-existence of a region in parameter space that (if existed) would lead to Hopf bifurcation or transcritical instability. Similarly, applying the numerical method to compute the partitioning curves under condition (23), it was shown that regions in parameter space exist for both Hopf and transcritical bifurcation. Parameters from Hopf bifurcation region as well as from Turing regions under both conditions on the domain size were shown to be in agreement with the theoretical prediction, when the system was numerically solved by using the finite element method. For each simulation the discrete L_2-norm of the successive time-step difference of the solutions is also given to visualise the temporal dynamics of the behaviour of the solutions during the convergence process. This work sets the premises to study more complex systems of non-autonomous reaction-diffusion equations during growth development whereby the parameter spaces are continuously evolving due to domain growth. It will be revealing to study how the Turing diffusion-driven parameter space, the Hopf and Transcritical regions evolve with time and how the dynamics of the model system evolve. The motivation for such extension is to find whether the conditions (23) and (34) for the domain size with reaction and diffusion rates continue to hold or whether a threshold for the domain size exists, beyond which, these conditions can be invalidated. Another direction of further investigation of the current work is to try and find similar relationships for different geometries such as spherical, elliptical and cylindrical domains. It may be noted that the eigenvalues and eigenfunctions of the Laplace operator change significantly depending on the boundary conditions and the geometry of the domain, therefore, application of the present method suggests, that finding similar condi-

tions for other geometries require a careful step-by-step procedure to find analogous conditions to those given by (23) and (34). It is also possible to apply the idea of the present work to the problems of pattern formation on bulk-surface geometries, where the relationship of surface area with reaction and diffusion rates can be explored to find the relevant influence of this relationship on the formation of spatial and/or temporal patterns. In [20] it is shown that the known condition of $d > 1$ is no longer necessary for pattern formation in the presence of linear cross-diffusion, which also provides a possible platform for the extension of the current work, to see, whether the invalidation of the condition $d > 1$ in the presence of linear cross-diffusion has any dependence with the relationship of reaction and diffusion rates with the domain size.

Acknowledgements

WS acknowledges support of the School of Mathematical and Physical Sciences Doctoral Training studentship. AM acknowledges support from the Leverhulme Trust Research Project Grant (RPG-2014-149) and the European Union's Horizon 2020 research and innovation programme under the Marie Sklodowska-Curie grant agreement No 642866. AM's work was partially supported by the Engineering and Physical Sciences Research Council, UK grant (EP/J016780/1). The authors (WS, AM) thank the Isaac Newton Institute for Mathematical Sciences for its hospitality during the programme (Coupling Geometric PDEs with Physics for Cell Morphology, Motility and Pattern Formation; EPSRC EP/K032208/1). AM was partially supported by a fellowship from the Simons Foundation. AM is a Royal Society Wolfson Research Merit Award Holder, generously supported by the Wolfson Foundation.

References

[1] Madzvamuse A, Chung AHW. The bulk-surface finite element method for reaction-diffusion systems on stationary volumes. J FE Anal Des 2015;108:0–21.
[2] Madzvamuse A, Chung AHW. Fully implicit time-stepping schemes and non–linear solvers for systems of reaction-diffusion equations. J App Math Comp 2014;244:361–74.
[3] Yan S, Lian X, Wang W, Upadhyay RK. Spatiotemporal dynamics in a delayed diffusive predator model. J App Math Comp 2013;244:524–34.
[4] Barreira R, Elliot CM, Madzvamuse A. The surface finite element method for pattern formation on evolving biological surfaces. Online J Math Biol 2011;29.
[5] Zhang R, Yu X, Zhu J, Loula AFD. Direct discontinuous Galerkin method for nonlinear reaction-diffusion systems in pattern formation. J App Math Mod 2014;38:1612–21.
[6] Madzvamuse A. Stability analysis of reaction-diffusion system with constant coefficients on growing domains. Int J Dyn Diff Eq 2008;1(4):250–62.
[7] Venkataraman C, Lakkis O, Madzvamuse A. Global existence for semilinear reaction-diffusion systems on evolving domains. J Math Biol 2012;64:41–67.
[8] Mackenzie JA, Madzvamuse A. Analysis of stability and convergence of finite difference method for a reaction-diffusion problem on a one dimensional growing domain. J Num Anal 2009;322(10):891–921.
[9] Madzvamuse A. Time-stepping schemes for moving finite elements applied to reaction -diffusion systems on fixed and growing domains. J Comp Phys 2006;214:239–63.
[10] Chaplain MAJ, Ganish M, Graham IG. Spatio-temporal pattern formation on spherical surfaces: numerical and application to solid tumour growth. J Math Biol 2001;42:387–432.
[11] Ghorai S, Poria S. Turing pattern incduced by cross-diffusion in a predator-prey system in presence of habitat complexity. J Chaos Solit Fract 2016;91:421–9.
[12] Henry BI, Wearne SL. Existence of turing instabilities in a two-species fractional reaction-diffusion system. SIAM J App Math 2007;62(3):870–87.
[13] Gierer A, Meinhardt H. A theory of biological pattern formation. Springer-Verlag Berlin; 1972. p. 30–9.
[14] Madzvamuse A, Maini PK, Wathen AJ. A moving grid finite element method applied to a model biological pattern generator. J Comp Phys 2003;190:478–500.
[15] Lengyel I, Epstein IR. A chemical approach to designing turing pattern in reaction-diffusion systems. Proc Natl Acad Sci USA 1992;89:3977–9.
[16] Ji K, Lee n, McCormick WD, Pearson JE. Experimental observation of self-replicating spots in a reaction-diffusion system. Nature 1994;369:215–18.
[17] Kim M, Bertram M, Pollmann M, Oertzen AV, Mikhialov AS, Rotermund HH. Controlling chemical turbulance by global delayed feedback: pattern formation in catalytic CO oxidation on pt(110). Science 18 May 2001;5520:891–921.
[18] Turing AM. The chemical basis of morphogenesis. Philos Trans R Soc Lond 1952;237:37–72.
[19] Lakkis O, Madzvamuse A, Venkataraman C. Implicit-explicit timestepping with finite element approximation of reaction-diffusion systems on evolving domains. SIAM J Num Anal 2014;51(4):2309–30.
[20] Madzvamuse A, Ndakwo HS, Barreira R. Stability analysis of reaction-diffusion models on evolving domains: the effect of cross-diffusion. Discr Cont Dyn Sys 2016;36(4):2133–70.
[21] Madzvamuse A, Maini PK. Velocity-induced numerical solutions of reaction-diffusion systems on continuously growing domains. J Comp Phys 2007;225:100–19.
[22] Schnakenberg J. Simple chemical reaction systems with limit cycle behaviour. J Theor Biol 1979;81:389–400. doi:10.1016/0022-5193(79)90042-0.
[23] Murray JD. Mathematical biology. Spatial models and biomedical applications. Springer New York; May 2013.
[24] Madzvamuse A, Chung AHW, Venkataraman C. Stability analysis and simulations of bulk-surface reaction-diffusion systems. Proc R Soc A 2015;471(10):891–921. 2014.0546
[25] Erneux T, Nicolis G. Propagating waves in discrete bistable reaction-diffusion systems. Phys D North-Holland 1993;67:237–44.
[26] Maini PK, Myerscough MR. Boundary-driven instability. J Appl Math Lett 1997;10(1):1–4.
[27] Madzvamuse A, Gaffney EA, Maini PK. Stability analysis of non-autonomous reaction-diffusion systems: the effect of growing domains. J Math Biol 2010;61:133–64.
[28] Iron D, Wei J, Winter M. Stability analysis of turing patterns generated by the schnakenberg model. J Math Biol 2003;49(4):358–90. doi:10.1007/s00285-003-0258-y.
[29] Larson MG, Bengzon F. The finite element method: theory, implementation and application. Texts in computational science and engineering. Springer. Verlag. Berlin Heidelberg; 2013.
[30] Baines MJ. Moving finite elements. Monographs on numerical analysis. Ox. Sc. Pub.; 1994.
[31] Xu C, Wei J. Hopf bifurcation analysis in a one dimension schnakneberg reaction-diffusion model. Nonlinear Anal Real World Appl 2012;13(4):1961–77.
[32] Yi F, Wei J, Shi J. Bifurcation and spatiotemporal patterns in a homogeneous diffusive predator-prey system. J Diff Eq 2009;265(5):1944–77.
[33] Yi F, Gaffney E, Lee S. The bifurcation analysis of turing pattern formation induced by delay and diffusion in the schnakenberg system. DiscreteCont Dyn Sys-B 2017;22(2):647–68.
[34] Liu P, Shi J, Wang Y, Feng X. Bifurcation analysis of reaction-diffusion schnakenberg model. Math Chem 2013;51:2001–19.
[35] Venkataraman C. Reaction-diffusion systems on evolving domains with applications to the theory of biological pattern formation. University of Sussex; 2011. Ph.D. thesis Dep. Math..
[36] Madzvamuse A, Maini PK, Wathen AJ. A moving grid finite element method for the simulation of pattern generation by Turing models on growing domains. J Sci Comp 2005;24(2).
[37] Keshet LE. Mathematical models in biology; classics in applied mathematics. Society for industrial and applied mathematics. Philadelphia. Pa. USA. (SIAM); 2005.
[38] Perko L. Differential equations and dynamical systems. 2nd ed. Springer, New York; 1996.
[39] Madzvamuse A. A numerical approach to the study of spatial pattern formation. University of Oxford; 2000. Ph.D. thesis Math. Inst. Oxofrd, UK.
[40] Smith IM, Griffiths DV. Programming the finite element method. second edition. Finite element method and data processing. John Wiley & Sons Ltd. New York; 1988.
[41] E. Campillo-Funollet, C. Venkataraman, A. Madzvamuse. A Bayesian approach to parameter identification with an application to Turing systems. 2016; https://arxiv.org/abs/1605.04718.